3 D POSITION OPTIMIZATION OF WIND TUNNEL GUIDE VANES FOR ACHIEVING UNIFORM FLOW

A Thesis

by

Aziz Mert Karul

Submitted to the
Graduate School of Sciences and Engineering
in Partial Fulfillment of the Requirements for
the Degree of

Master of Science

in the
Department of Mechanical Engineering

Özyeğin University
September 2024

3 D POSITION OPTIMIZATION OF WIND TUNNEL GUIDE VANES FOR ACHIEVING UNIFORM FLOW

Approved by:

Associate Professor Özgür Ertunç, Advisor
Dept. of Mechanical Eng.
Özyeğin University

Assistant Professor Altuğ M. Başol
Dept. of Mechanical Eng.
Özyeğin University

Associate Professor Nilay Sezer Uzol
Dept. of Aerospace Eng.
Middle East Technical University

Date Approved: August 9, 2024

To my family and my dear friends

ABSTRACT

This study aims to optimize the placement of guide vanes to achieve a uniform velocity distribution at the wind tunnel corner outlet while minimizing the impact of secondary flow, a critical consideration in fluid dynamics applications. By employing two objective functions that are minimizing the standard deviation of wall shear stress on the outer wall and reducing velocity gradient at the outlet, the research addresses key factors that influence system efficiency and durability. The methodology involved both two-dimensional and three-dimensional simulations. Initially, two-dimensional optimizations were conducted to identify promising design seeds, which were subsequently employed in more comprehensive three-dimensional analyses. This approach allowed for a thorough exploration of the design space and used the efficiency of two-dimensional studies to guide the more complex three-dimensional simulations. The findings from these simulations were substantial. The optimized designs demonstrated a marked improvement in flow uniformity and a significant reduction in the impacts of secondary flow when compared to baseline designs. This indicates that strategic placement of guide vanes can effectively streamline the flow, enhancing the overall performance of the system. Moreover, the inclusion of wall shear stress as an optimization parameter was particularly revealing. It was observed that optimizing for wall shear stress not only improved the distribution of velocity but also had the added benefit of reducing energy losses. The significance of incorporating wall shear stress alongside velocity uniformity cannot be overstated. These findings have broad applicability across various systems that utilize guide vanes, such as wind tunnels, pipe systems, and other flow regulation devices. Achieving a uniform flow and minimizing secondary effects are important for these systems to perform at their best.

The insights gained from this study can thus be instrumental in designing more efficient and durable flow systems, contributing to advancements in fields ranging from aerospace engineering to industrial fluid dynamics.

ÖZETÇE

Bu çalışma, akışkanlar dinamiği uygulamalarında kritik bir konu olan, çıkışta eşit bir hız dağılımı elde etmek ve ikincil akışın etkisini en aza indirmek amacıyla kılavuz kanatların yerleşiminin optimize edilmesini hedeflemektedir. Bu araştırma, sistem verimliliğini ve dayanıklılığını etkileyen önemli faktörleri ele alarak, iki hedef fonksiyon kullanmıştır: duvar kayma gerilmesinin standart sapmasını minimize etmek ve ikincil akış etkilerini azaltmak. Metodoloji hem iki boyutlu hem de üç boyutlu simülasyonları içermektedir. Başlangıçta, iki boyutlu optimizasyonlar gerçekleştirilmiş ve bu tasarımlar daha kapsamlı üç boyutlu analizlerde kullanılmıştır. Bu yaklaşım, tasarım alanının detaylı bir şekilde incelenmesini sağlamış ve bu iki boyutlu çalışmaların hesaplama verimliliği, daha karmaşık üç boyutlu simülasyonları bilgilendirmek için kullanılmıştır. Bu simülasyonların bulguları oldukça önemlidir. Optimize edilmiş kılavuz kanat tasarımları, akış eşitliliğinde belirgin bir iyileşme ve ikincil akış etkilerinde önemli bir azalma göstermiştir. Bu, kılavuz kanatların stratejik yerleştirilmesinin akışı etkili bir şekilde düzenleyebileceğini ve sistemin genel performansını artırabileceğini göstermektedir. Ayrıca, optimizasyon parametresi olarak duvar kayma gerilmesinin dahil edilmesi özellikle açıklayıcı olmuştur. Duvar kayma gerilmesi için yapılan optimizasyonun, hız dağılımını iyileştirmenin yanı sıra yüzey aşınmasını ve enerji kayıplarını da azalttığı gözlemlenmiştir. Duvar kayma gerilmesinin hız eşitliliği ile birlikte ele alınmasının önemi küçümsenemez. Yaklaşım, sistem verimliliğini ve ömrünü doğrudan etkileyen daha bütüncül bir optimizasyon çerçevesi sunmaktadır. Kayma gerilmesinin azaltılmasıyla, sistem zaman içinde daha az mekanik aşınma yaşar ve bu da bakım maliyetlerini düşürür ve operasyonel ömrü uzatır. Bu bulgular, kılavuz kanatları kullanan çeşitli

sistemlerde geniş bir uygulama alanına sahiptir, örneğin rüzgar tünelleri, boru sistemleri ve diğer akış düzenleme cihazları. Bu sistemlerin en iyi performansı göstermesi için eşit bir akış dağılımı elde etmek ve ikincil etkileri en aza indirmek çok önemlidir. Bu çalışmadan elde edilen içgörüler, havacılık mühendisliğinden endüstriyel akışkan dinamiğine kadar çeşitli alanlarda daha verimli ve dayanıklı akış sistemlerinin tasarımında etkili olabilir.

ACKNOWLEDGEMENTS

I would like to extend my deepest gratitude to my advisor Özgür Ertunç, whose guidance, expertise, and encouragement have been invaluable throughout this research. Your insightful feedback and unwavering support have been instrumental in shaping this work.

I am also immensely grateful to Alper Akardere, who camaraderie, collaborative spirit, and constructive discussions have enriched this journey. Your shared knowledge and willingness to help have made this experience both productive and enjoyable. I would like to sincerely thank Altuğ Melik Başol and İsmail Arı for their assistance with HPC usage.

Finally, I wish to express my heartfelt thanks to my family. Your constant support, patience, and belief in me have been my greatest source of strength. Your love and encouragement have been a cornerstone throughout this endeavor, and I am forever grateful for your unwavering faith in my abilities.

TABLE OF CONTENTS

LIST OF TABLES

LIST OF FIGURES

LIST OF NOMENCLATURE

C	Chord length of the airfoil, p. 9.
C_{loss}	Pressure loss coefficient, p. xiii.
$ConViol_j$	The amount by which the j^{th} constraint is violated., p. 31.
C_{SKE}	Secondary kinetic energy, p. 28.
d_i	The distance range within each vane, p. 23.
k	Turbulent kinetic energy, p. 12.
$LinW_{obj}^{2D,3D}$	Linear weight of the each objective, p. 31.
μ	Dynamic viscosity, p. 12.
N	The number of data points, p. 28.
N_{con}	Number of constraints for the objectives, p. 31.
N_{obj}	The total number of objectives, p. 31.
$Norm_i$	Normalization value, p. 31.
$Norm_j$	Normalization value for the constrains, p. 31.
$\mathbf{n}_{vane}$	Number of vane, p. 9.
Obj_i	Response value for the design, p. 31.
ω	Specific dissipation rate, p. 12.
$\overline{P_{S,out}}$	Mass flow averaged outlet static pressure, p. 29.
$\overline{P_{T,in}}$	Mass flow averaged inlet total pressure, p. 29.
P	Pressure, p. 12.
$QuadCon_j$	Quadratic weight for the constrains, p. 31.
ρ	Density, p. 12.
$\rho\overline{u_i u_j}$	Reynolds stresses, p. 12.
S	The diagonal distance from the inner to the outer radius of the corner, p. 9.
σ_{τ_w}	Standard deviation of wall shear stress, p. 27.

τ_{ij}	Viscous stress tensor, p. 12.
τ_w	Wall shear stress, p. 27.
θ	Angle of airfoil, p. 24.
U	Velocity of the fluid, p. 12.
V_{bulk}	Bulk velocity, p. 29.
x_{ci}	Center of origin of each vane, p. 24.
x_i	Final positions of each vane,, p. 26.
y	The distance from the wall, p. 19.

CHAPTER I

INTRODUCTION

In various flow systems, including wind tunnels, flow test systems, compressors, and turbines, vane-like devices are employed to regulate the flow direction. These structures are especially significant at corners where they influence the system's efficiency and performance. High-temperature heat transfer in turbines can impact the lifespan of materials and the overall performance of the turbine. In flow test systems for automobiles, combustion chambers, turbines, compressors, or heat exchangers, corner design typically equipped with vanes is crucial to maintaining high-quality flow. The goal is to generate uniform flow without turbulence, flow separation, secondary flow effects, and pressure or density variations. In high-temperature environments, vane-like devices contribute to improved heat transfer by maintaining steady flow patterns. They help in distributing heat more evenly across the turbine components, which is critical for efficient thermal management and reducing hot spots that could lead to material degradation[1].

1.1 Importance of Corners in Closed-Loop Wind Tunnels

A closed-loop wind tunnel requires four corners to divert the flow around the loop. However, these corners result in substantial pressure reduction, thus reducing the efficiency and effectiveness of the wind tunnel. Corners are particularly crucial due to the increased dynamic pressure, which significantly contributes to the overall losses. These four corners are responsible for almost % 50 of the overall pressure loss [2]. Guide vanes reduce losses at corners and maintain a consistent velocity profile[2][3][4]. It has been observed that the inclusion of guide vanes in structures that rotate the

flow by 90 degrees leads to a substantial decrease in pressure loss. These observations are corroborated by both empirical and computational fluid dynamics (CFD) investigations. It was emphasized that the impact of secondary flow is diminished, flow stability is enhanced, and achieving a homogeneous flow at the outlet region is necessary by increasing the number of vanes [5].The design of corners in flow systems significantly impacts the overall flow characteristics. Properly designed corners with vanes help minimize flow separation and reduce the formation of vortexes. This results in a more uniform flow distribution and reduces turbulence, which is essential for accurate testing and reliable performance data[6].

1.2 Design of Vanes

Vanes are commonly made from thin sheet metal, which is appropriate for most tunnel sizes. However, when dealing with larger tunnels that must endure high pressures, it is preferable to use thick airfoil-section vanes, even if they only provide a modest aerodynamic benefit compared to thinner ones [7]. The shape and alignment of the vanes are crucial since they significantly influence the quality of flow and the amount of pressure loss. The selection of airfoil is crucial for evaluating flow quality. Several crucial elements that influence the performance of the vane were found: chord length, thickness-to-chord ratio, shape, curvature, profile, and the number of vanes [8]. The main objective is to reduce pressure drop, which can be achieved by choosing a vane section with a high lift-to-drag ratio. This ensures that the airfoil produces substantial lift while minimizing drag. The use of high lift enhances the effectiveness of flow redirection, while low drag minimizes the pressure decrease at the corners [9]. It is crucial to maintain a low level of resistance to motion and a high level of smoothness in the fluid movement. To achieve this, it is compulsory to avoid the separation of the boundary layer [9].

1.3 Reducing Corner Losses

By regulating the flow parameters that cause pressure loss, it is possible to decrease corner losses. Turbulent flows are commonly observed in reality, adding complexity to the flow characteristics. After the corner's entrance, the main flow speed reduces, resulting in the formation of secondary whirling flow caused by variations in radial pressure distribution and centrifugal forces. The swirling motion gives rise to a pair of counter-rotating vortices, commonly referred to as Dean vortices[10]. Moreover, the curved wall on the outer side affects the flow by creating unfavorable pressure differences in the nearby area. At elevated Reynolds numbers, the flow transitions into an unstable state characterized by the formation of shearing layers. This causes the release of secondary flows and the creation of stationary vortices. Increased velocity variations in separated areas were noted Hence, by inducing rotational motion in the flow around the corner without any separation, it is possible to achieve a consistent and even flow at the outlet of the corner[11]. Achieving uniform flow is crucial in various applications, including wind tunnels and compressors. Vane-like structures play a key role in ensuring uniformity by directing the flow and minimizing fluctuations. This leads to more accurate simulation environments in wind tunnels and efficient performance in compressors and turbines[6].

1.4 Secondary Flow Effects

Secondary flow is the movement of fluid particles at a right angle to the main flow direction. The major flow channel governs the overall fluid flow, while secondary flow emerges due to factors such as the free stream area's geometry, boundary conditions, and other influences. Secondary flow effects at wind tunnel corner were examined quantitatively using the k -ϵ model [12]. In a previous study, numerical calculations were used to simulate the existence of corner vortices that disturb the main flow[13]. A separate investigation analyzed the characteristics of secondary flow in 90-degree

rotating duct configurations at various Mach values [14]. Secondary flow effects were prevalent in these experiments. Due to the 90-degree rotating duct configurations in the corners of the wind tunnel, secondary flow effects are common. By using airfoil-shaped guide vanes in the wind tunnel, the negative impacts of secondary flow can be minimized. Although it is not possible to eliminate secondary flow effects completely, it is possible to significantly diminish them by improving the design. A study conducted using numerical methods found that separations in the guiding vanes can be minimized through appropriate design techniques [15].The vane-like structures regulate flow direction by creating secondary flows and reducing turbulence in systems like turbines and compressors. These devices help manage the primary stream wise flow and maintain uniform flow distribution, reducing pressure loss and enhancing performance [1]. Vane-like structures are effective in reducing turbulence by stabilizing the flow and preventing the formation of large vortices. This is particularly important in high-speed flows where turbulence can lead to significant energy losses and mechanical stress on the system components[1][16].

1.5 Position Optimization of Vane Position in Closed-Loop Wind Tunnels

The current work goes beyond simple optimization of spacing by considering both the quantity and arrangement of vanes in closed-loop wind tunnel corners. The objective of this study is to optimize guide vane placement designs by considering secondary flow data, aiming to produce a uniform velocity distribution and reduce pressure losses at the closed loop wind tunnel corner. Thorough optimization efforts are crucial for improving the performance and efficiency of wind tunnel testing facilities.

In closed-loop wind tunnels, the spacing between the corner's guide vanes are usually set to be the equally; however, this does not always lead to consistent flow downstream of the vanes. Therefore, optimization techniques were used to identify the most advantageous placement of guide vanes at the corners of a wind tunnel.

The objective is to reduce the distance between the vanes and corners while maintaining a consistent distribution of velocity downstream of the vanes at the corner outlet. The optimization targets are specified as the standard deviation of wall shear stress on the corner outer surface and the sum of the squared gradients of the major velocity component in the transverse direction at the outlet. A computational fluid dynamics (CFD) program was utilized for conducting 2-D and 3-D flow simulations and optimization.

1.6 Open Fields in the Literature

A review of the literature reveals a notable gap in the investigation of the effects of guide vane arrangements on performance. Specifically, there has been a lack of studies addressing the placement of guide vanes in the design of closed-loop wind tunnels. It is crucial to examine how these placements affect the flow profile at the outlet. Furthermore, in closed-loop wind tunnel designs, particularly in three-dimensional studies of corner parts, there is a lack of research on optimizing guide vane positions to achieve a uniform flow while minimizing secondary flow effects.

1.7 Hypothesis of the Study

Guide vanes are used for regulate the flow in the channels. The usage of guide vanes in 90-degree bends and channels has been discussed; however, a detailed analysis of secondary flow effects and the flow distribution at the outlet region is crucial. Proper alignment and positioning of the guide vanes can mitigate secondary flows and ensure a more uniform outlet flow distribution, thereby enhancing the overall efficiency and performance of the system. The placement of guide vanes significantly impacts these factors.

1.8 Objective of this Study

The objectives of this study are as follows:

- Perform detailed two-dimensional and three-dimesional aerodynamic simulations to determine an optimal guide vane position configuration.
- Utilize advanced two and three-dimensional optimization techniques to investigate two and three-dimensional effects on the guide vane position arrangement.
- Innovate an optimization approach that targets both the attainment of uniform velocity distribution in the corner outlet region and the mitigation of flow separations and secondary flow effects, without decreasing overall aerodynamic performance.

1.9 Methodology

Two-dimensional Computational Fluid Dynamics analyses are frequently utilized for preliminary design studies and optimization processes that prioritize computational efficiency. However, for scenarios involving complex geometries or requiring precise predictions of flow behavior, three-dimensional CFD analyses are indispensable. Despite the inherent complexities and computational demands of 3D analyses, the initial 2D results provide valuable insights and design inputs that expedite the subsequent 3D optimization process. Consequently, 3D geometries can be optimized more efficiently by leveraging preliminary 2D analysis data.

In this study, the application of CFD is critical for optimizing the placement of vane-like structures within a wind tunnel. The optimization was conducted using the Simcenter Star-CCM+ design manager, focusing on positioning vanes at the wind tunnel corners. Key parameters, such as the placement and angles of attack of the vanes, were allowed to vary within predefined limits. The primary objective was to achieve a uniform velocity distribution at the wind tunnel corner outlet. The optimization process was facilitated by the Simcenter Star-CCM+ software, which incorporates the SHERPA algorithm, a method specifically designed for optimization tasks.

By employing both 2D and 3D CFD analyses and utilizing the SHERPA algorithm within Simcenter Star-CCM+, this study achieved a streamlined and effective optimization process. The findings highlight the critical role of advanced optimization algorithms in enhancing the performance and reliability of vane-like structures in flow systems.

CHAPTER II

NUMERICAL APPROACH

2.1 Geometry

The wind tunnel design for Özyeğin University employs a corner contraction, drawing inspiration from seminal works by Barlow, Rae, and Pope (1984), as well as Mehta and Bradshaw (1979). This strategic design choice aims to enhance the efficiency of the testing area within the closed loop wind tunnel. The specific dimensions and layout of this design are depicted in Figure 2. A critical aspect of corner design is the formation of vortices at the corners, characterized by the rotational movement of airflow around these edges. These vortices are significantly influenced by both the shape of the corner and the prevailing flow conditions. To mitigate and manage these vortices, various forms of guide vanes—ranging from thin sheet metals to meticulously arranged airfoils—are employed at these corners.

Airfoil-shaped guiding vanes play a crucial role in reducing the formation of specific types of vortices, such as tip leakage vortices and hub wall passage vortices. The design proposed by Sahlin and Johansson in 1991 is recognized as particularly effective for the airfoil shapes used in the vanes of closed-loop wind tunnel corners. Sahlin's publication underscores the efficiency of this design, which is illustrated in Figure 1. The airfoil coordinates for the guide vane are provided in Appendix A. Additionally, Figure 2 provides a detailed representation of the corner's shape, dimensions and width, as well as the precise positioning of the vanes.Figure 3 shows the inlet and outlet dimension of tunnel corner.

Further refinement in vane design and placement comes from the work of Li, Chen, and Wu (2023), who developed equations to determine the optimal number

and spacing of airfoil vanes. Their research focused on optimizing vane placement to mitigate secondary flow effects, and they derived Eq. 1 for this purpose. In Eq. 1, S represents the diagonal distance from the inner to the outer radius of the corner, and C is the chord length of the airfoil. For instance, with S measured at 3455 mm and C at 1000 mm, their calculation suggests an optimal vane count of 6.34. Consequently, this study chosen for 6 vanes based on this calculation.

$$n_{vane} = 2.14 \left(\frac{S}{C} \right) - 1 \tag{1}$$

Two-dimensional studies were conducted using dimensions of 2835 mm for the entrance and 2370 mm for the outflow, ensuring accurate simulation of airflow characteristics. The three-dimensional simulations further refined the analysis, establishing an axis length of 2370 mm. The inlet is characterized by a square shape, while the outlet adopts a rectangular shape, allowing for a detailed examination of the flow dynamics.

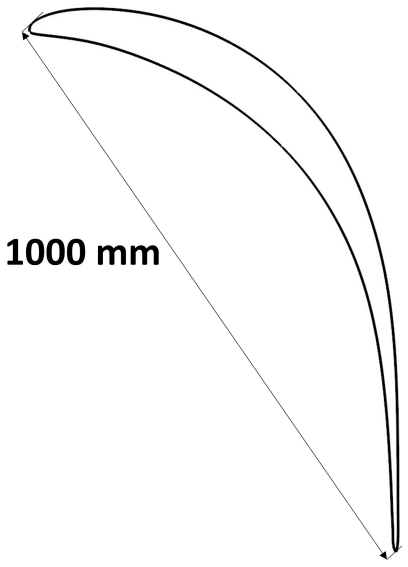

Figure 1: Airfoil Vane Drawing

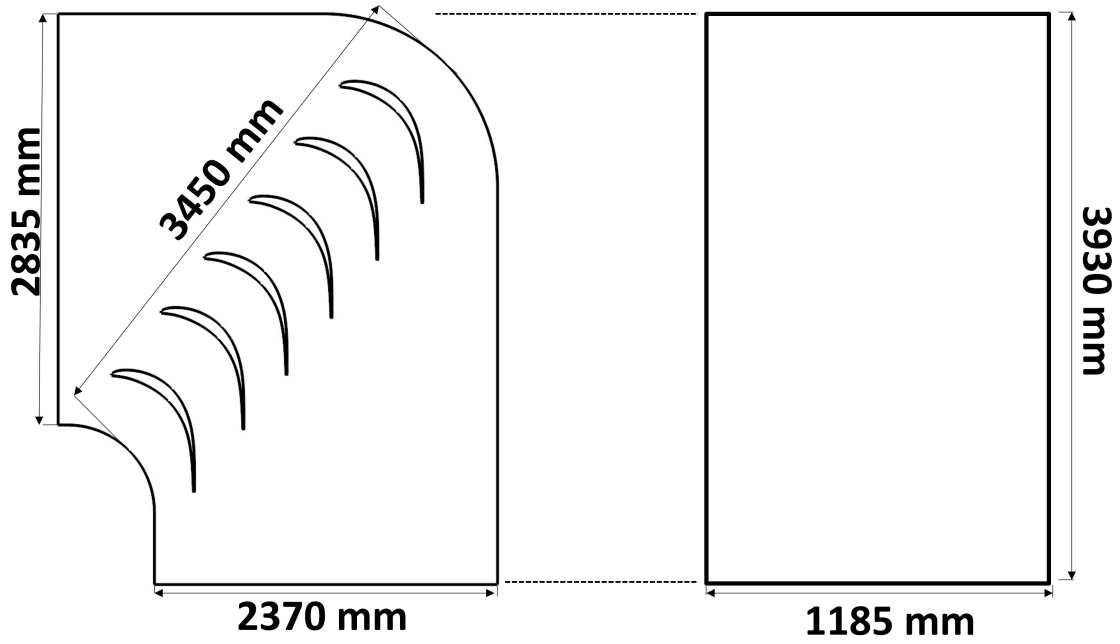

Figure 2: Half section corner drawing and dimensions with six vane placed

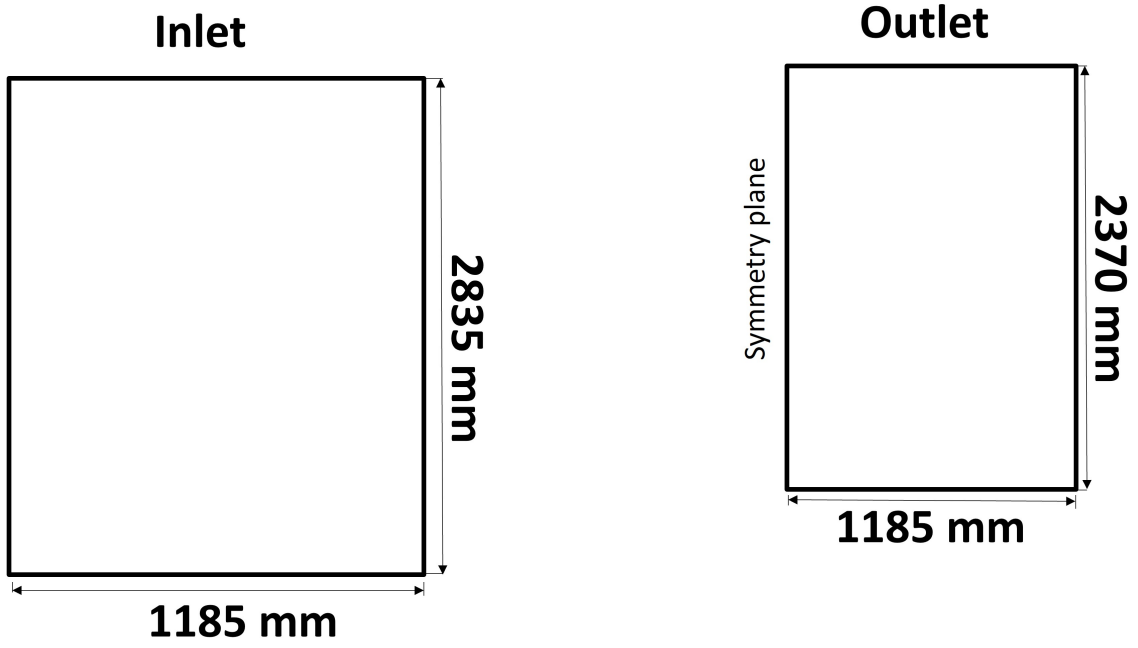

Figure 3: Half section inlet and outlet dimensions

The comprehensive design and strategic placement of airfoil vanes are critical for

optimizing the wind tunnel's performance, reducing pressure losses, and ensuring accurate testing conditions. By meticulously considering the geometric dimensions and flow characteristics, this design approach provides a robust framework for advanced aerodynamic testing and research.

2.2 Numerical Set-Up and Physical Models

2.2.1 Governing Equations

The analysis was conducted utilizing the k-ω SST (Shear Stress Transport) turbulence model, a robust approach combining the strengths of both the k-ϵ and k-ω models to improve near-wall treatment and accurately predict the onset and behavior of turbulence in various flow regimes. This model effectively leverages the unrestricted flow characteristics inherent in the k-ϵ turbulence model, enhancing its performance by transitioning to the k-ω formulation in regions close to the wall. The k-ϵ model is primarily employed in the outer boundary layer to handle the free-stream turbulence accurately.

This enhancement is achieved by transforming the k-ϵ model into the k-ω formulation, incorporating additional modifications. The key differentiation between this novel formulation and the original k-ω model is the integration of a cross-diffusion term into the ω equation, along with adjustments to the modeling constants. These changes aim to improve the model's accuracy in capturing turbulence phenomena near the wall while preserving the beneficial attributes of the k-ϵ model in the outer boundary layer regions.

The Reynolds averaged Navier-Stokes equations used in this analysis are derived from the fundamental principles of fluid dynamics, namely the conservation of mass and momentum for incompressible and statistically stationary turbulent flow [17].

Conservation of Mass:

$$\frac{\partial \overline{U_i}}{\partial x_i} = 0 \tag{2}$$

U is the velocity of the fluid.

Momentum Equation:

$$\rho \overline{U_j} \frac{\overline{U_i}}{\partial x_j} = -\frac{\partial \overline{P}}{\partial x_i} + \frac{\partial}{\partial x_j}\left(\mu \frac{\partial \overline{U_i}}{\partial x_j} - \rho \overline{u_i u_j}\right) \tag{3}$$

In this equation, U_i represents the velocity of the free stream, ρ is the density, P is the pressure, and μ is the dynamic viscosity. The term $\mu \frac{\partial \overline{U_i}}{\partial x_j}$ corresponds to the viscous stress tensor τ_{ij}, and $\rho \overline{u_i u_j}$ represents the Reynolds stresses, which account for the effects of turbulence.

Original k-ω Model Equations:

The original k-ω model equations are expressed as follows[18]:

Turbulent Kinetic Energy (k) Equation:

$$\frac{D\rho k}{Dt} = \tau_{ij} \frac{u_i}{x_j} - \beta^* \rho \omega k + \frac{\partial}{\partial x_j}\left[(\mu + \sigma_{k1}\mu_t)\frac{k}{x_j}\right] \tag{4}$$

$$\frac{D\rho k}{Dt} = \frac{\partial \rho k}{\partial t} + U_j \frac{\partial \rho k}{\partial x_j} \tag{5}$$

In a statistically stationary flow, the local time derivative of any quantity is zero, $\frac{\partial \rho k}{\partial t} = 0$.

$$u_j \frac{\partial(\rho k)}{\partial x_j} = \tau_{ij} \frac{u_i}{x_j} - \beta^* \rho \omega k + \frac{\partial}{\partial x_j}\left[(\mu + \sigma_{k1}\mu_t)\frac{k}{x_j}\right] \tag{6}$$

Specific Dissipation Rate (ω) Equation:

$$\frac{D\rho\omega}{Dt} = \frac{\gamma}{\nu_t} \tau_{ij} \frac{u_i}{x_j} - \beta^* \rho \omega^2 k + \frac{\partial}{\partial x_j}\left[(\mu + \sigma_{w1}\mu_t)\frac{\omega}{x_j}\right] \tag{7}$$

$$\frac{D\rho\omega}{Dt} = \frac{\partial \rho\omega}{\partial t} + U_j \frac{\partial \rho\omega}{\partial x_j} \tag{8}$$

In a statistically stationary flow, the local time derivative of any quantity is zero, $\frac{\partial \rho\omega}{\partial t} = 0$.

$$u_j \frac{\partial(\rho\omega)}{\partial x_j} = \frac{\gamma}{\nu_t}\tau_{ij}\frac{u_i}{x_j} - \beta^*\rho\omega^2 + \frac{\partial}{\partial x_j}\left[(\mu + \sigma_{w1}\mu_t)\frac{\omega}{x_j}\right] \tag{9}$$

In these equations:

- $\sigma_{k1} = 0.85$
- $\sigma_{w1} = 0.5$
- $\beta_1 = 0.0750$
- $\beta^* = 0.09$
- $\gamma_1 = \frac{\beta_1}{\beta^*} - \frac{\sigma_{w1}k^2}{\sqrt{\beta^*}}$ [19]

These constants and terms are crucial for accurately capturing the turbulent behavior and ensuring that the model provides reliable predictions across different flow regimes. The modifications introduced in the k-ω SST model enhance its applicability and accuracy, making it a valuable tool for studying complex turbulent flows in engineering and scientific applications[19].

2.2.1.1 Mesh Sensitivity

A study was carried out to examine the influence of mesh sensitivity on a two-dimensional. An investigation of mesh sensitivity was performed using the 6-vane design. The placements of the vanes remained constant, and investigations were conducted at each of these places. The aim of this study is to identify the optimal mesh size prior to commencing the optimization phase, with the goal of minimizing computational time.

Numerous numerical analyses are conducted by employing different base mesh sizes until the residual of Y-momentum reaches a satisfactory threshold of 1e-5. The initial velocity of the item when it reached the corner was 20 m/s. The distance between the vanes was constant.

Research was done utilizing eight different base mesh sizes. The pressure loss values and the distribution of outflow velocity were obtained from this research and depicted visually. The data shown in Table 1 demonstrates that the fundamental mesh size achieved convergence at a value of 0.025 meters. This suggests that the results were rather consistent and did not show significant deviations above this threshold. The pressure drop between 0.025 and 0.015 m is less than % 1. In Figure 4 pressure drop values according to number of cells are shown.

Table 1: Mesh Sensitivity Number of Cells and Pressure Loss Table

Base Mesh Size	*Number of Cells*	*Pressure Loss*
0.15	18,941	25.5
0.12	25,394	24.7
0.1	32,484	23.7
0.08	44,809	22.4
0.05	87,426	21.2
0.025	267,660	19.1
0.015	649,753	19.2
0.012	959,237	19.2

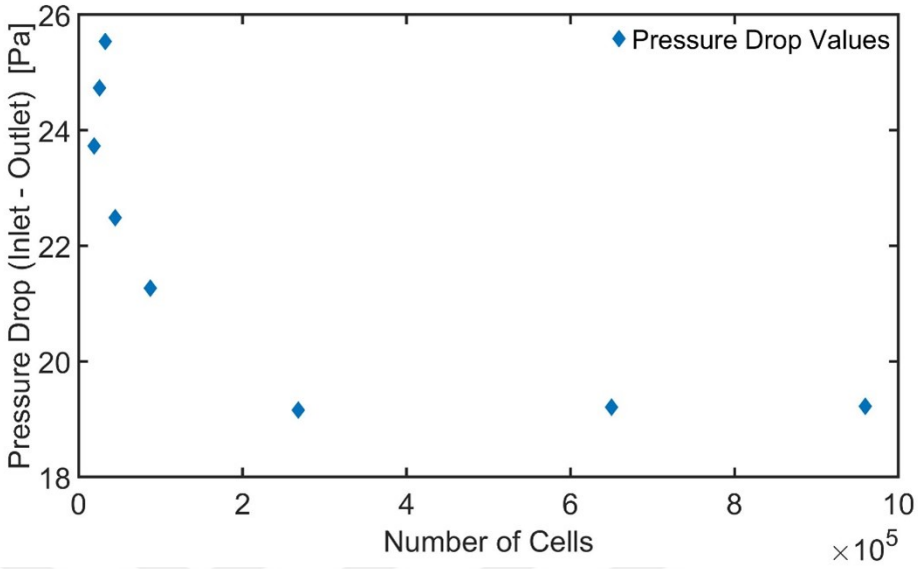

Figure 4: 2 D pressure drop for different base mesh size.

As shown in Figure 5, a line probe was defined at the wind tunnel corner outlet. The line probe was created by narrowing the prism layer regions near the walls, where the flow is expected to be zero. Consequently, the flow distributions in Figure 6 do not approach zero near the walls.

Figure 6 illustrates the velocity distribution for different base mesh sizes. This graph depicts the influence of mesh resolution on the velocity distribution and the level of precision in the solution.

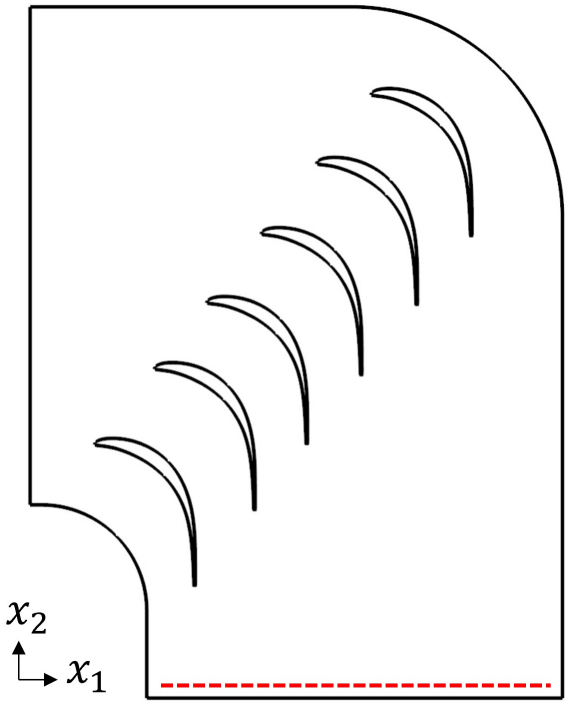

Figure 5: Corner outlet line probe

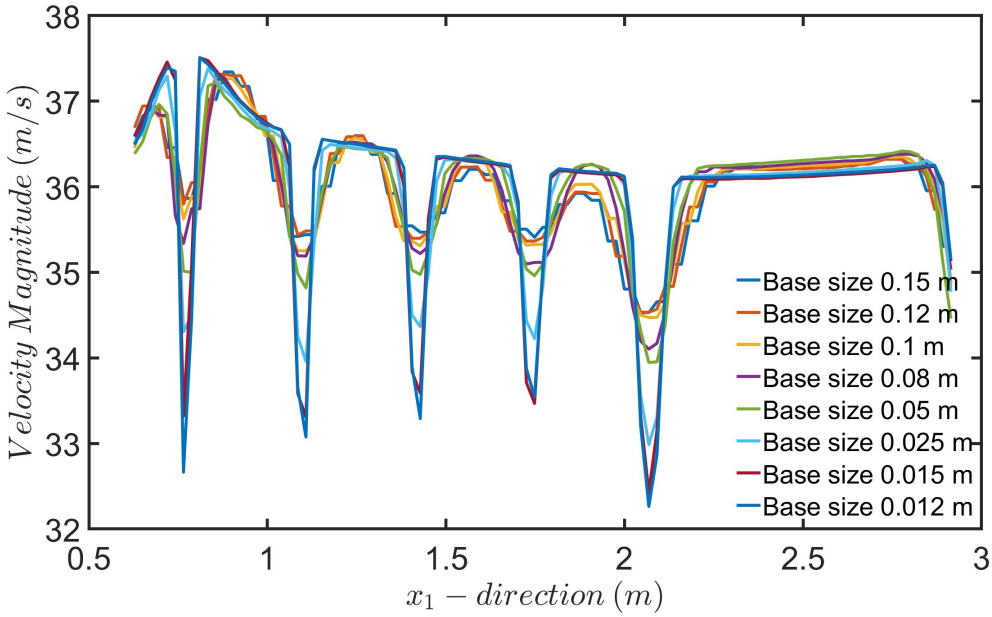

Figure 6: Corner outlet velocity distribution for different base mesh sizes (Left side is inner corner, Right side is outer corner)

To achieve optimal resolution of the flow around the airfoil walls and outer corners, six prism layers are selected. In Table 2 features of the meshes are mentioned. The fluid's behavior is more complex in areas that are next to walls. In some regions, slower flow velocity can cause viscosity to have a stronger impact. In order to enhance the accuracy of simulating the fluid behavior in close proximity to the wall, a prism layer is integrated into the model [20]. Therefore, as seen in Figure 7, a prism layer meshes around the guide vanes is available. The study emphasizes the importance of airflow after the trailing edges of the airfoil guide vanes which shown in the Figure 8. To accurately capture this phenomenon, a finer grid is used in this area. In contrast, a coarser mesh is applied in the intake section to reduce computational time, as shown in Figure 9.

Table 2: Features of the Mesh

Parameter	**Value**
Selected Base Mesh Size	0.025 [m]
Maximum Cell Size	0.025 [m]
Minimum Cell Size	0.0025 [m]
Number of Prism Layers	6 [-]
Prism Layer Total Thickness	0.005 [m]
First Prism Layer Thickness	0.00083 [m]
Total Number of Cells Around the Single Vane	865 [-]

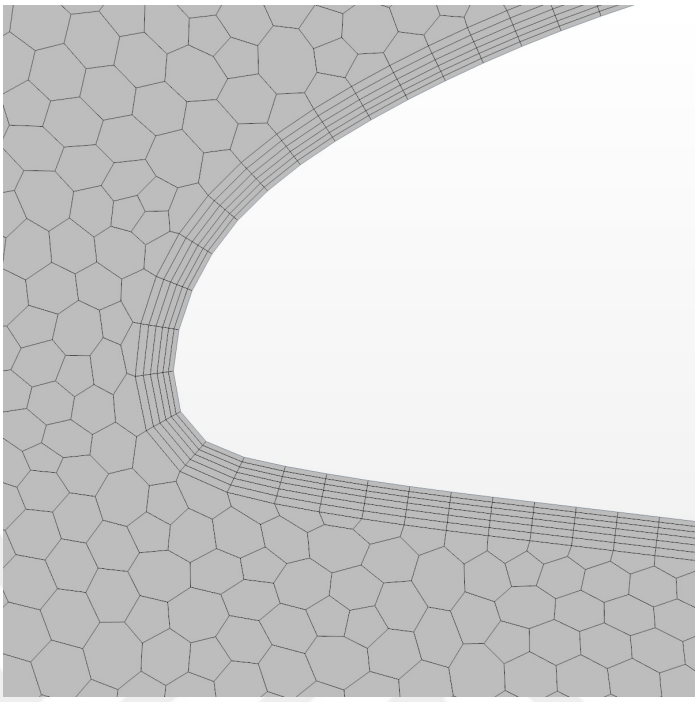

Figure 7: Detailed prism layer meshes around the leading edge of the airfoils guide vanes

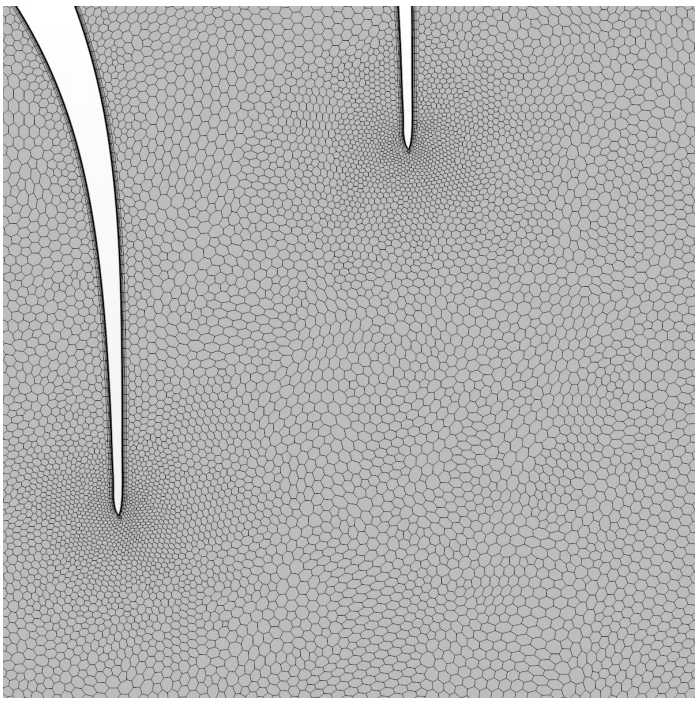

Figure 8: Trailing edge mesh scene for airfoil guide vanes

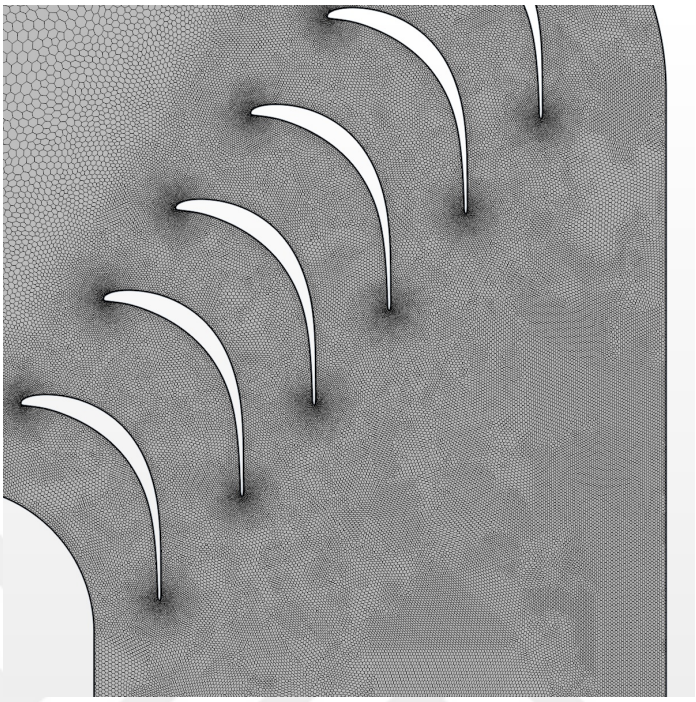

Figure 9: Mesh scene of the corner

A typical method involves characterizing the area next to the wall by employing dimensionless variables, which are defined by the particular conditions near the wall. The variable y represents the orthogonal distance from the wall. The dimensionless wall distance, shown as $y+$, may be precisely expressed as

$$y^+ = \frac{y\rho u}{\mu} \tag{10}$$

The variables in the equation are defined as follows: y represents the distance from the wall to the beginning point on the grid, ρ represents the density of the fluid, u represents the fluid velocity immediately above the wall, and μ represents the dynamic viscosity of the fluid[20]. The objective of this is to accurately depict the boundary layer in close proximity to the wall. The all-wall treatment utilizes a blend of wall functions that simulate the low-wall treatment for small grids and the high-wall treatment for large grids. The primary objective of this system is to provide coherent answers for grids with moderate resolution, especially when the central point of the

wall cell falls inside the buffer zone of the border layer. This offers a wall treatment that is appropriate for a broad spectrum of near-wall mesh densities. The analysis revealed that the wall's y^+ value varied between 0 and 1 for 2 dimensional case, as seen in Figure 10.

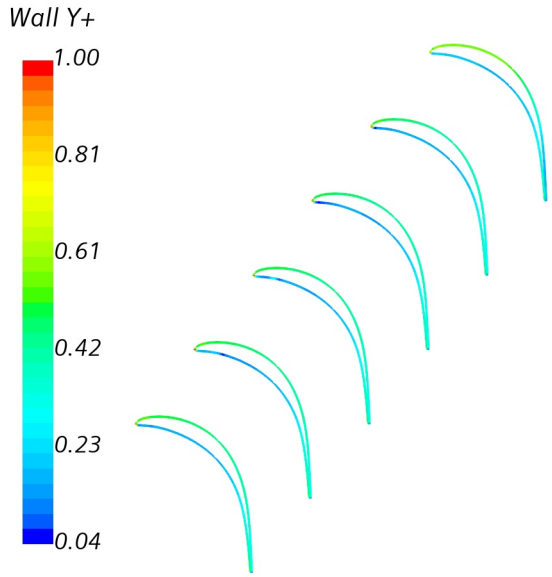

Figure 10: Wall y+ value on two dimensional airfoil vane

For the three-dimensional analyses, the wall $y+$ values, as shown in Figure 11, were examined. The employed wall functions are capable of resolving these values, and it is evident that the buffer region has been avoided[21]. This ensures that the wall functions are operating effectively.

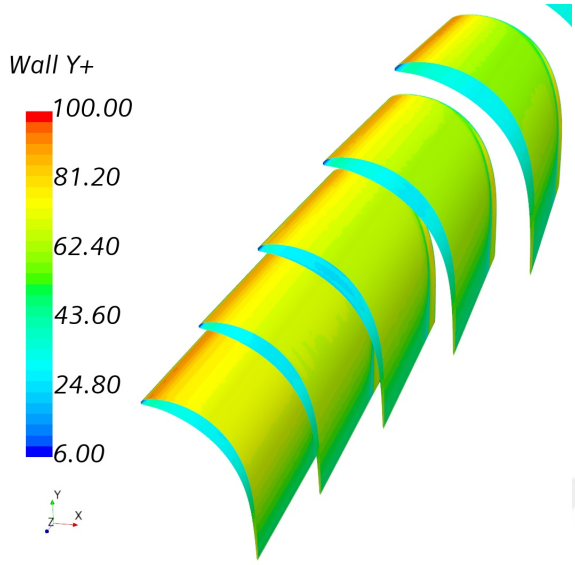

Figure 11: Wall y+ values on three dimensional airfoil vane

CHAPTER III

OPTIMIZATION

The Sherpa algorithm is an optimization method that emphasizes two critical parameters: efficiency and robustness. The results demonstrated that SHERPA outperformed other algorithms, showcasing superior performance in both efficiency and robustness. SHERPA's strength lies in its ability to integrate local and global search strategies effectively, enabling it to adapt seamlessly to diverse optimization scenarios [22].

Figure 13 displays the revised coordinate system utilized for describing the positions of the vanes and their associated names, which are essential elements of the design parameters. The new coordinate system which is shown in the Figure 12, is defined based on the inner and outer radii of the corner. After the establishment of a new coordinate system, the vanes were arranged according to their separate positions along the x-axis of that coordinate system. In the first stage, the distances between the guiding vanes are equal. The design requirements provided instructions on the particular intervals and distances at which the placements should be adjusted. However, it is essential to establish some restrictions on the x-axis. The goal of these restrictions was to prevent the vanes from overlapping. To prevent any potential overlap or interference during the optimization process of organizing, certain distribution intervals were specified. The intervals are provided in Table 4, with a fixed increase of 0.01 meters. Each vane has its own unique center of origin point. These items are positioned at the origin in their respective coordinate planes. The optimization parameters are shown in Table 4.

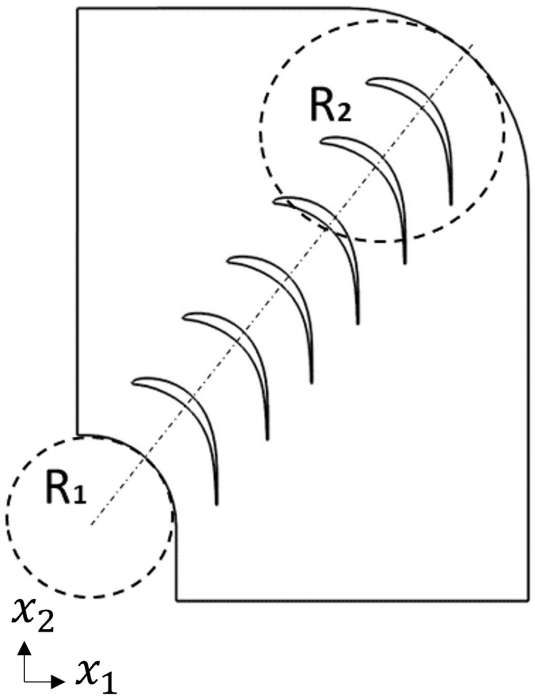

Figure 12: New coordinate system for vane placement

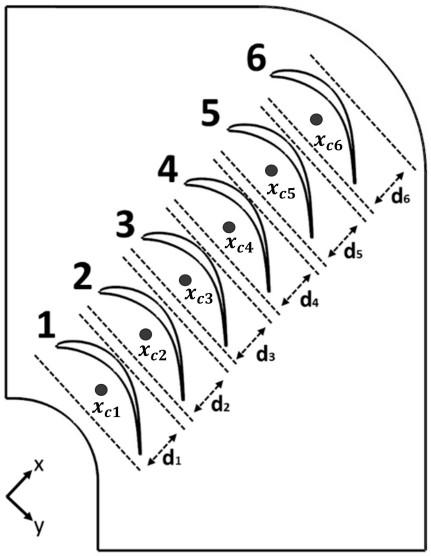

Figure 13: Vane numbering of closed-loop wind tunnel corner part

As depicted in Figure 13, the d_i values denote the distance range within each

vane can vary, extending from -0.2 to +0.2 meter. According to this representation, the origin points of each vane can be determined as $\frac{d_i}{2}$. Initially, all vanes are positioned with equal interval in the wind tunnel corner. To provide a more detailed understanding, the x_{ci} values, representing the origin of each vane, are shown in Figure 13. x_{ci} coordinates are represented in the Table 3

Table 3: Each airfoil vane center of origins

	x coordinate	y coordinate
x_{c1}	0.663	0.45
x_{c2}	0.969	1.222
x_{c3}	1.275	1.608
x_{c4}	1.582	1.993
x_{c5}	1.888	2.379
x_{c6}	2.194	2.765

The value of the angle θ is illustrated as 0 "zero" degrees in Figure 14. The angle variation is performed relative to leading edge of the airfoil, which is also depicted in Figure 14. The initial value of 106 degrees, used for optimization, is shown in Figure 14 as a name of $\theta_{initial}$. The airfoil coordinates for the guide vane are provided in Appendix A.

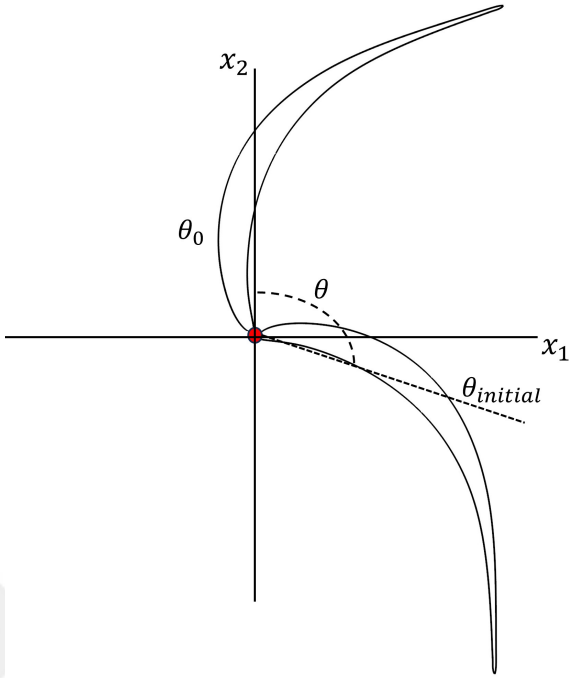

Figure 14: Airfoil guide vane θ angles and representation

Table 4: Input Parameters

Variable	Position Range	Increment
θ	100° to 112°	0.1 deg
d_1	-0.1 to 0.2 m	0.01 m
d_2	-0.2 to 0.2 m	0.01 m
d_3	-0.2 to 0.2 m	0.01 m
d_4	-0.2 to 0.2 m	0.01 m
d_5	-0.2 to 0.2 m	0.01 m
d_6	-0.2 to 0.2 m	0.01 m

3.1 Vane Distribution Equation

The distribution of the vanes on the corner after optimization is represented by Eq. 11.

$$x_i = x_{ci} \overset{+}{-} \frac{d_i}{2} \tag{11}$$

The variables x_i represent the final positions of each vane, where x_1 to x_n correspond to individual vanes. The variables x_{ci} represent the center of origin for each vane, denoted as x_{c1} to x_{cn}. The variables d_i represent the position range distance resulting from the optimization phase, denoted as d_1 to d_n.

3.2 Constraints and Design Requirements

The constraints were determined based on the pressure drop and the residuals of Y-momentum. These constraints prevent the removal of unfavorable conditions during the optimization phase and slow down progress, potentially resulting in less effective outcomes. If the residual of the Y-momentum exceeds 1e-4, then the simulation is considered to be in an unstable condition. Therefore, it was deduced that the residual Y-momentum was below 1e-4. According to the Bernoulli equation, an increase in the velocity of a fluid flow results in a reduction in the fluid's pressure. Since the corner section of the wind tunnel is designed to act as a nozzle corner, it is imperative to enhance the velocity of the airflow near the outlet. Therefore, it is crucial in this situation to ensure that the pressure difference between the inlet and outlet flows always stays above zero.

$$\text{Constraints} = \begin{cases} y_{\text{momentum}} < 10^{-4} \\ \text{Pressure Drop} > 0 \end{cases} \tag{12}$$

3.3 Multi-Objective Optimization

The positioning of the corner section's vane was determined through the use of multi-objective optimization. Two objective functions were designed to address the possibility of encountering challenging situations that cannot be handled by a single objective. A study was performed to analyze the velocity gradients at the outlet of

the wind tunnel corner section. The outlet of the corner was employed to ensure a uniform and steady distribution of flow along the x-axis for two dimensional simulation. In three dimensional optimization the aim was to achieve a uniform and steady flow distribution in the corner outlet plane. This plane is defined by the x and z axes. The square of the sum of the partial derivative of the average velocity component u_2 with respect to y, $\sum \left(\frac{\partial \overline{u_j}}{\partial y}\right)^2$, was calculated because the outlet region in 2D simulations and optimizations is perpendicular to the y-axis in the coordinate plane. However, because the gradient was mostly negative, it was essential to apply the squaring operation to this equation. Since the aim of this study is to minimize fluctuations in the flow profile, whether it is negative or positive does not affect the results of this study. The choice was taken to minimize the sum of these gradients as the objective function. In the 3D optimization phase, an extra objective function is utilized. This is because the flow profile show variation in two axes. Therefore, it is essential to take into account the summation of the square of the partial derivative of $\overline{u_2}$ with respect to z. Due to the specific attributes of the flow, the flow will be almost insignificant in areas adjacent to the wall. The formation of a boundary layer will lead to unfavorable consequences in the equation, since it restrain the uniform distribution of flow. In order to do this, a line probe was deployed at a precise distance of 0.01 m from each side of the outlet walls for two dimensional optimization. In three-dimensional optimization, the corner outlet plane was constrained by walls. Point probes, consisting of the X and Z axes, were used.

The standard deviation σ_{τ_w}, as defined in Eq. 13, was used as the second objective function. It was calculated by taking the square root of the average squared difference between each individual value τ_w and the mean value $\overline{\tau}_w$, and then dividing by the total number of values N. The value of σ_{τ_w} was determined using wall shear stresses from the outer wall of corner which is shown in Figure 15. The term σ_{τ_w} represents the magnitude of fluctuations in the wall shear stress that a fluid encounters when

flowing across a surface. The aim was to minimize the standard deviation σ_{τ_w}, which is computed as the square root of the average of the squared differences between each τ_{wi} and the mean value $\overline{\tau}_w$.

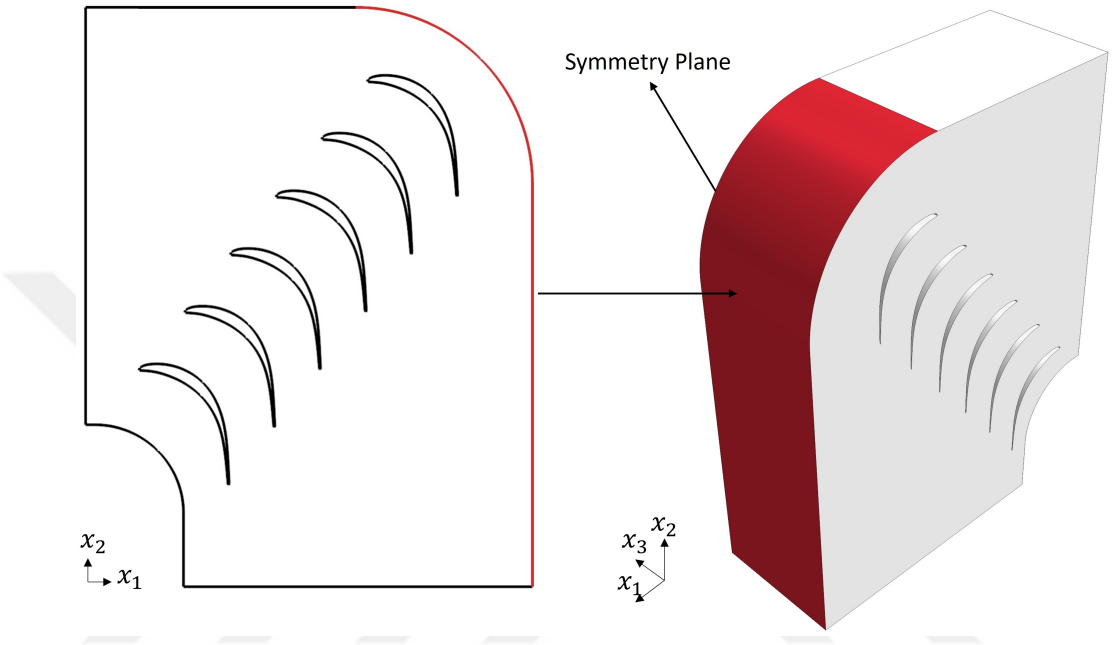

Figure 15: Outer wall of the wind tunnel corner representation (Red lines and region)

$$\text{Minimize} \quad \sigma_{\tau_w} = \sqrt{\frac{1}{N}\sum_{i=1}^{N}(\tau_{wi} - \bar{\tau}_w)^2} \tag{13}$$

In this study, N represents the number of data points, which can indicate either position. The symbol τ_{wi} denotes specific values of wall shear stress, whereas $\overline{\tau}_w$ indicates the mean wall shear stress.

3.4 Secondary Kinetic Energy and Flow Loss Coefficients

The full examination of flow zones is performed to accurately compute the secondary flow. This allows for the creation of a coefficient Eq. 14 that accurately captures the secondary kinetic energy over the whole system. C_{SKE} uses as a practical indication for evaluating the extent of this phenomenon in different circumstances. Furthermore,

it is utilized as an objective function to minimize its value in optimization techniques [23].

$$C_{SKE} = \frac{\frac{1}{2}\rho\overline{V_{sec}^2}}{\overline{P_{T,in}} - \overline{P_{S,in}}} \tag{14}$$

This equation defines the coefficient of secondary kinetic energy (C_{SKE}), which represents the ratio of the average kinetic energy associated with secondary flows to the difference between the mass flow average total pressure at the inlet $\overline{P_{T,in}}$ and the mass flow average static pressure at the inlet $\overline{P_{S,out}}$. It provides insight into the amount of energy contained in the secondary flow relative to the available pressure energy.

$$V_{bulk} = \begin{pmatrix} \overline{V_x} \\ \overline{V_y} \\ \overline{V_z} \end{pmatrix} \tag{15}$$

The bulk velocity vector (V_{bulk}) is a three-dimensional representation of the mass flow average velocity components in the x, y, and z directions. Each component ($\overline{V_x}$, $\overline{V_y}$, and $\overline{V_z}$) is the mass flow averaged velocity in the respective direction, comprising the overall motion of the fluid[23].

$$V_{sec} = V - \left(\frac{V \cdot V_{bulk}}{|V_{bulk}^2|}\right) V_{bulk} \tag{16}$$

The secondary velocity C_{SKE} is the velocity component of a fluid element that remains after subtracting the component of the velocity that is aligned with the bulk velocity (V_{bulk}). This represents the deviation from the bulk flow, showing how individual particles move relative to the mass flow average flow direction.

These secondary flows occur due to various forces acting on the fluid, such as centrifugal forces in curved channels or boundary layer effects near solid surfaces.

They are essential for understanding the non-uniform flow patterns that can develop in complex fluid systems.

$$C_{loss} = \frac{\overline{P_{T,in}} - P_{T,out}}{\overline{P_{T,in}} - \overline{P_{S,out}}} \tag{17}$$

This equation defines the coefficient of pressure loss (C_{loss}), which quantifies the pressure loss between the inlet and outlet of a system relative to the available pressure difference between the mass flow average total pressure at the inlet ($\overline{P_{T,in}}$) and the mass flow average static pressure at the outlet ($\overline{P_{S,out}}$). It indicates the efficiency of the system in terms of energy loss due to factors such as friction or turbulence.

3.5 Objective Functions

The following objective functions are defined for 2D and 3D optimizations:

$$\text{Minimize} \quad W_{obj}^{2D} = \begin{Bmatrix} \sum \left(\frac{\partial U_j}{\partial x}\right)^2 \\ \sigma_{\tau_w} = \sqrt{\frac{1}{N}\sum_{i=1}^{N}(\tau_{wi} - \bar{\tau}_w)^2} \end{Bmatrix} \tag{18}$$

$$\text{Minimize} \quad W_{obj}^{3D} = \begin{Bmatrix} \sum \left(\frac{\partial U_j}{\partial x}\right)^2 + \sum \left(\frac{\partial U_j}{\partial z}\right)^2 \\ \sigma_{\tau_w} = \sqrt{\frac{1}{N}\sum_{i=1}^{N}(\tau_{wi} - \bar{\tau}_w)^2} \\ C_{loss} \end{Bmatrix} \tag{19}$$

CHAPTER IV

RESULTS

In the context of Design Manager, the efficiency of a design is assessed based on how well it achieves the set objectives and the extent to which it adheres to established constraints. A key characteristic of a high-performance design is its ability to not only meet but exceed all constraints while achieving a positive evaluation for its objectives.

Any design that satisfies the requirements that have been provided is allowed to proceed regardless of the degree to which it adheres to those limits. When all of the restrictions have been accomplished, the only thing that has a numerical influence on the performance evaluation is the objectives. It is possible to calculate the performance value of any design by applying the equation that is presented below:

$$\sum_{i=1}^{N_{obj}} \frac{LinW_{obj}^{2D,3D} \cdot (-1) \cdot Obj_i}{Norm_i} - \sum_{j=1}^{N_{con}} \frac{QuadCon_j \cdot ConViol_j^2}{Norm_j^2} \tag{20}$$

The variable N_{obj} represents the total number of objectives, $LinW_{obj}^{2D,3D}$ represents the linear weight of the each objective, "-1" for objectives that are minimized, The response value for the design's ith objective is denoted by the variable Obj_i. The normalization value that you enter for the ithobjective is denoted by the variable $Norm_i$. The number of constraints discovered in the design investigation is denoted by the variable N_{con}, while the weight $QuadCon_j$ represents the weight for the jth constraint that is quadratic. The variable $ConViol_j$ represents the extent to which the jth constraint is violated, whereas the variable $Norm_j$ represents the value of the constraint itself, normalized to reflect the jth constraint. Whenever the constraint value is zero, the normalization value is equal to one.

4.1 Two dimensional position optimization results

Both the angle of airfoil and the vane placements for the optimum design are displayed in Table 5. 1000 iterations were carried out in order to optimum the position. It was the 763rd iteration that produced the most beneficial solution, which is depicted in Figure 16 with a blue diamond symbol. The initial version of the design is represented by a red squared. In Figure 16, the ideal combination of minimizing the sum of velocity gradient, which is depicted by a yellow diamond, and minimizing the standard deviation of the wall shear stress, which is depicted by a green diamond, is displayed. Also Figure 17 shows the velocity distribution for three different optimum results which are, optimum, optimum with minimum velocity gradient summation on the outlet region of wind tunnel corner and optimum with minimum standard deviation of wall shear stress on the outer wall.

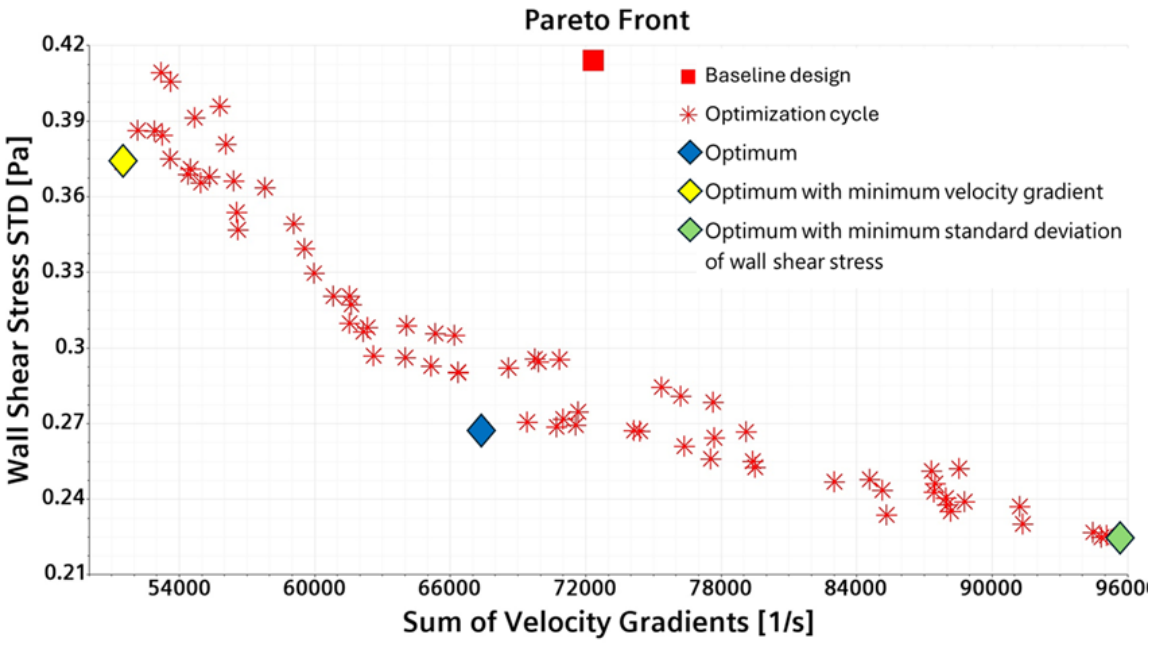

Figure 16: Two dimensional optimization pareto plot

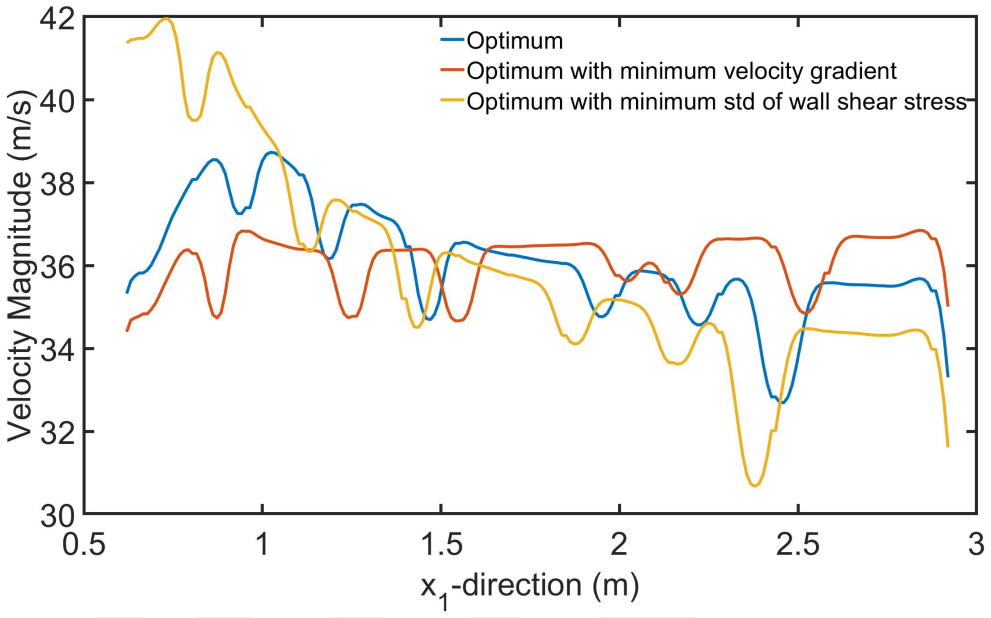

Figure 17: Outlet velocity distributions of various optimum designs on the Pareto front(Left side is inner corner, Right side is outer corner)

Table 5: Initial and 2-D optimized vane positions and angle of airfoil

	Initial	2-D Optimized
Airfoil Angle (°)	105	110.7
x_1 (m)	0	0.11
x_2 (m)	0	0.01
x_3 (m)	0	-0.03
x_4 (m)	0	0.19
x_5 (m)	0	0.15
x_6 (m)	0	0.01

The optimized results are superimposed in Figure 18 to facilitate a comparison between the placements of the initial and the optimum results. A total of 1000

optimizations were performed. Throughout the optimization process, the optimal positions and angle of airfoil vanes were identified, with the red vanes representing these locations.

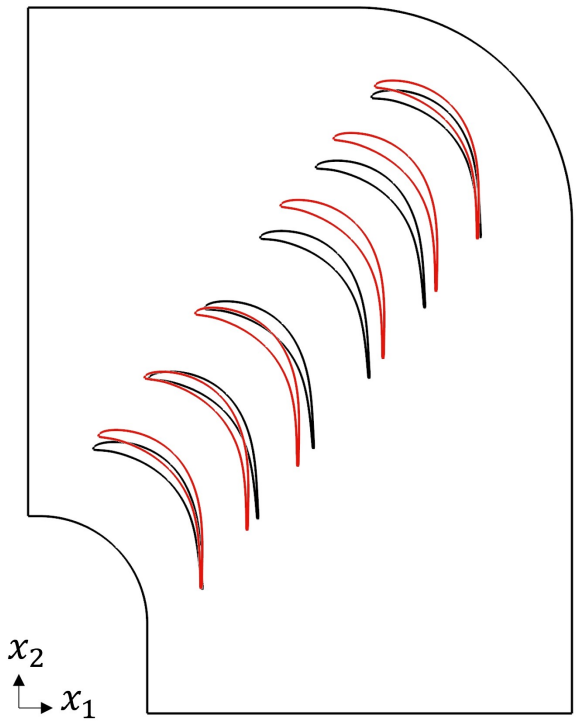

Figure 18: Vane Position Distribution comparison between Initial and Optimized (Red Lines) Design

The employment of two optimization functions, $\sigma_{\tau_w} = \sqrt{\frac{1}{N}\sum_{i=1}^{N}(\tau_{wi} - \overline{\tau}_w)^2}$ and $\sum\left(\frac{\partial \overline{u_2}}{\partial x}\right)^2$, leads to the following outcomes.The velocity distribution at the outlet was both even and free from separations. A comparison was made between the best values for minimizing $\sum\left(\frac{\partial \overline{u_2}}{\partial x}\right)^2$ and the objective of reducing $\sigma_{\tau_w} = \sqrt{\frac{1}{N}\sum_{i=1}^{N}(\tau_{wi} - \overline{\tau}_w)^2}$, which was a key parameter used during the optimization process.

The second parameter ensures that the velocity distribution at the wind tunnel

corner outlet remains constant. However, even though the optimal value of $\sum \left(\frac{\partial \bar{u}_2}{\partial x}\right)^2$ creates a uniform velocity distribution, it also causes separations due to the vanes being positioned close to each other. Similarly, when examining the minimization and optimal value of $\sigma_{\tau_w} = \sqrt{\frac{1}{N}\sum_{i=1}^{N}(\tau_{wi} - \bar{\tau}_w)^2}$, another key parameter, it becomes evident that the flow distribution is not uniform. By combining these two objective function, a solution was found that reduces both the non uniform velocity and the separation.

The initial design velocity distribution is shown in Figure 19. In this figure, separations occur at the trailing edge of the number 6 airfoil guide vane, which is closest to the outer wall. Adjusting the angle of airfoil vane (θ) does not prevent this separation. However, as shown in Figure 20, the separation is eliminated in the optimized design velocity distribution.

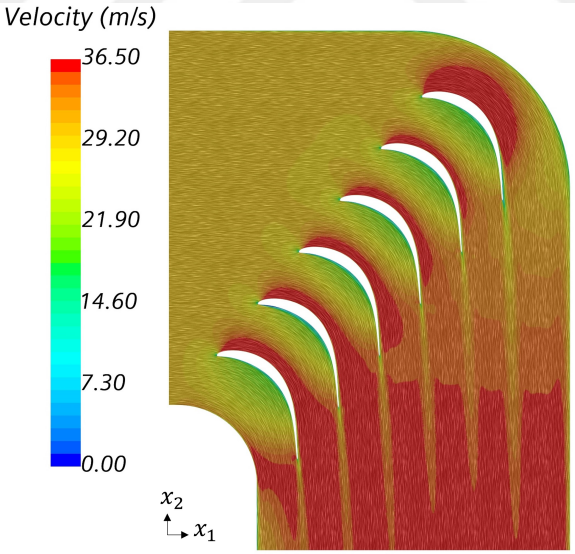

Figure 19: Two dimensional velocity distribution scene for initial design

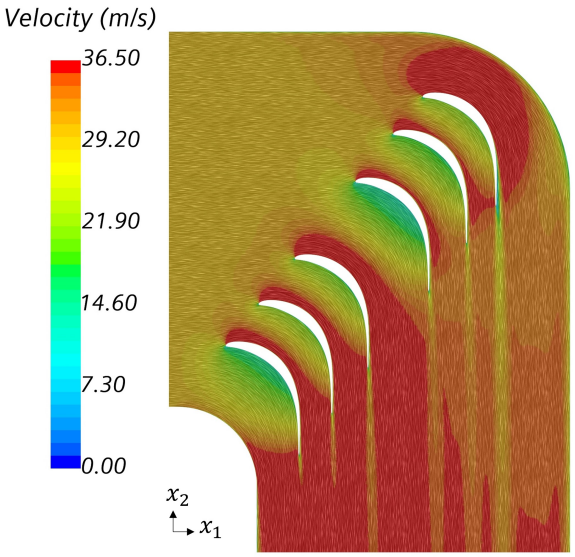

Figure 20: Two dimensional velocity distribution scene for optimum result

As shown in Figure 21, the diagram that is referred to as "2D Initial and 2D optimum design outlet velocity distribution" is provided. The original distribution as well as the optimum velocity distribution are both depicted here. Compared to equally distributed airfoil guide vane placement velocity distribution, the optimal result suggests a more uniform velocity distribution at the wind tunnel corner outlet region.

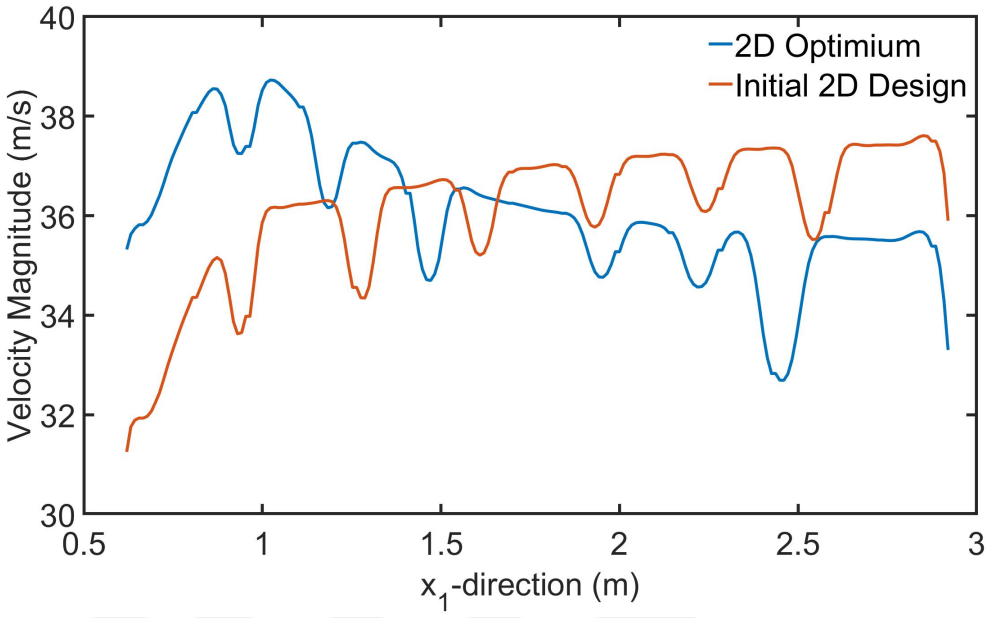

Figure 21: Initial and optimum design outlet velocity distribution(Left side is inner corner, Right side is outer corner)

4.2 Three dimensional position optimization results

In fluid dynamics, understanding three-dimensional flow structures, 22 is crucial, especially in complex engineering applications involving sudden changes in flow direction, such as in 90-degree corner turns. The behavior of 3D flow is often characterized by the interaction between the primary flow, which follows the intended path, and secondary flows, which arise due to geometric constraints, abrupt directional changes, and the interaction of boundary layers. Secondary flow phenomena are particularly significant in such scenarios, as they can lead to energy losses, increased drag, and undesirable flow separation. In the context of a corner turn with airfoil guide vanes, secondary flows typically emerge as vortices and swirl patterns that deviate from the primary flow direction, resulting in non-uniform velocity distributions and increased wall shear stresses. These effects can degrade the performance of fluid systems by promoting flow separation, leading to inefficiencies. The challenge lies in designing

systems that minimize secondary flow effects through careful optimization of geometry, such as altering the angle of airfoil vanes and spacing between guide vanes. By employing computational fluid dynamics optimization, engineers can visualize these 3D flow structures and iteratively refine designs to achieve uniform flow distribution and reduce secondary flow impacts, thereby enhancing the overall performance and efficiency of fluid transport systems.

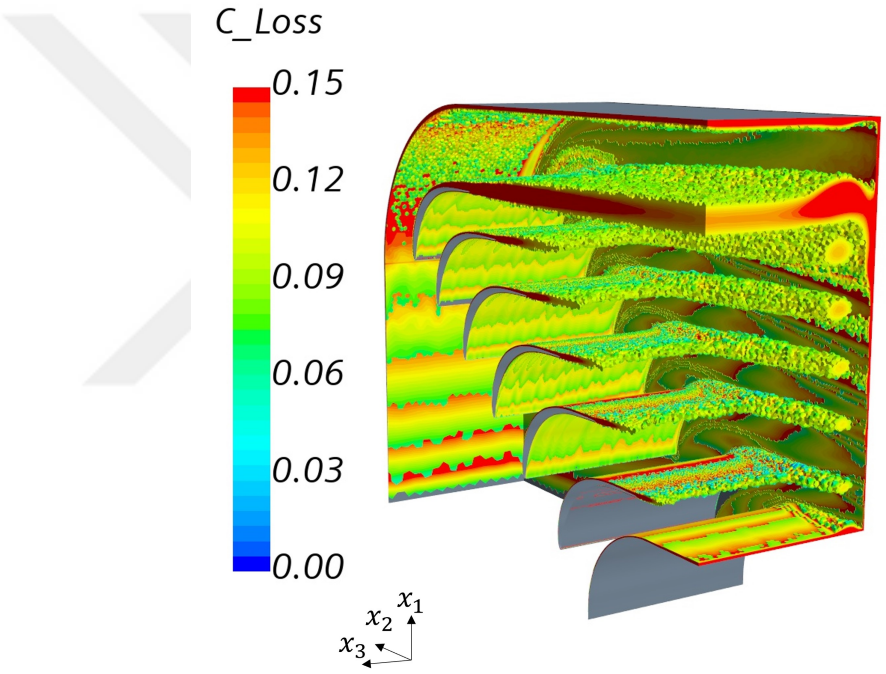

Figure 22: Visualization of 3D Flow Structure C_{loss} Threshold

The design seed for the three-dimensional position optimization was obtained by selecting the top 100 designs from the two-dimensional optimization process before beginning the three-dimensional optimization process. Through the course of this research, secondary flow structures that were previously undetectable in two dimensions were discovered. Additionally, there was a continuous flow through the vanes that did not exhibit any separation, and the implications of secondary flow were identified and

mitigated.500 three dimensional position optimization was done. Table 6 represents the whole number of design for each 2D and 3D optimization process. A workstation is used with 32 cores was utilized. The total duration for the three-dimensional optimization process was 960 hours. A design simulation was completed every 1.92 hours.

Table 6: Total optimization design counts

	2-D Optimization	3-D Optimization
# of design	1000	500

Three axes were used to prepare the Pareto front since there are three objective functions. Exhibited in Figure 23, the three axes yield ideal results. Table 7 below displays these findings and designs. Moreover, Figure 24 also displays the velocity distributions. The best result from the optimization is also included in Table 8, based on performance estimates.

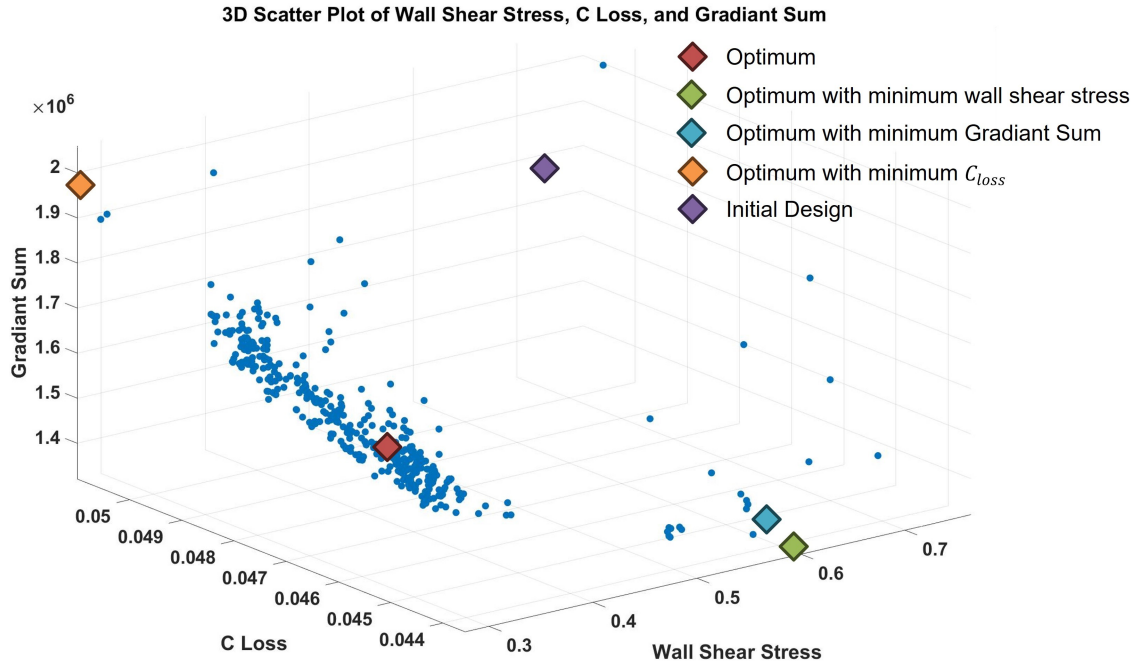

Figure 23: Three Dimensional Pareto Plot

Table 7: 2D optimum design and 3D optimum design vane positions

	3D optimum design	2D optimum design
AoA (°)	109.1	110.7
d_1 (m)	0.12	0.11
d_2 (m)	0.18	0.01
d_3 (m)	0.19	-0.03
d_4 (m)	0.20	0.19
d_5 (m)	0.20	0.15
d_6 (m)	0.15	0.01

The vane position in the two-dimensional design, the vane position in the three-dimensional optimum design Table 7 was also observed. The flow pattern in the mid-plane is depicted in Figure 24 after conducting a three-dimensional study. Adjusting

the placements of the guide vanes periodically has a negligible effect on the flow distribution in the middle section. However, significant differences develop in the impacts of these secondary flow patterns when they are taken into account.

Table 8: Vanes and Angle of Attack Values for Optimum Results

	Initial Design	C Loss Optimum Perf.	Wall Shear Std. Dev. Optimum Perf.	Gradient Sum Optimum Perf.	Best Perf. for Three Obj.
Vane 1	0	0.16	0.09	0.1	0.12
Vane 2	0	0.17	0.2	0.16	0.18
Vane 3	0	0.2	0.2	0	0.19
Vane 4	0	0.19	0.12	0.19	0.2
Vane 5	0	0.2	0.2	0.18	0.2
Vane 6	0	0	0.15	-0.02	0.15
AOA	108	107.7	110	107.7	109.1

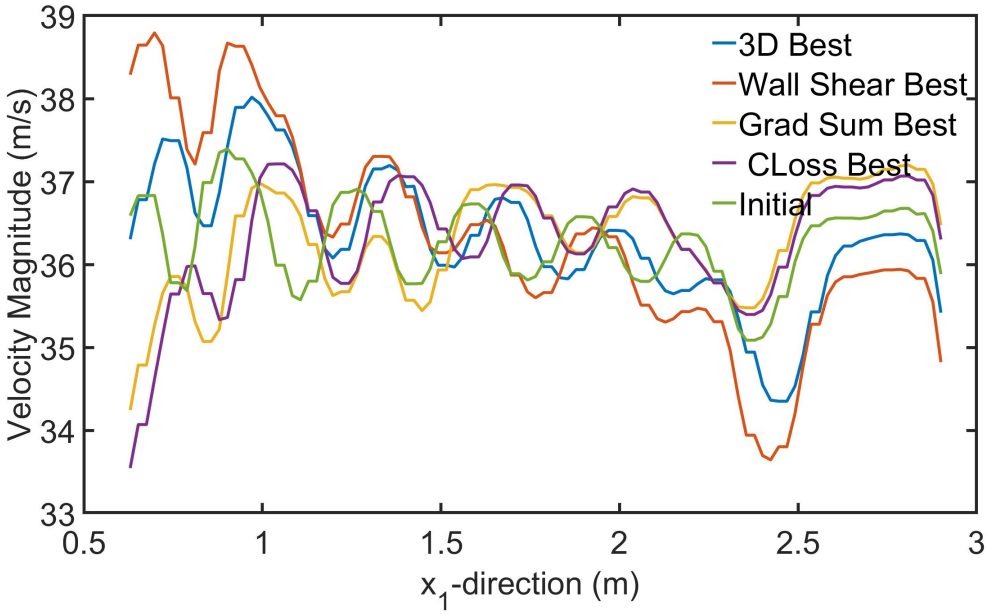

Figure 24: Three-dimensional velocity distribution for optimum, optimum with standard deviation of wall shear stress,optimum with gradient summation, optimum with C_{loss}, initial design (Left side is inner corner, Right side is outer corner)

The vane distributions for the initial design, two-dimensional optimization, and

three-dimensional optimization are illustrated in Figure 25 The black airfoil guide vanes represent the initial design, the red ones correspond to the two-dimensional optimization, and the blue airfoil guide vanes indicate the results of the three-dimensional optimization.

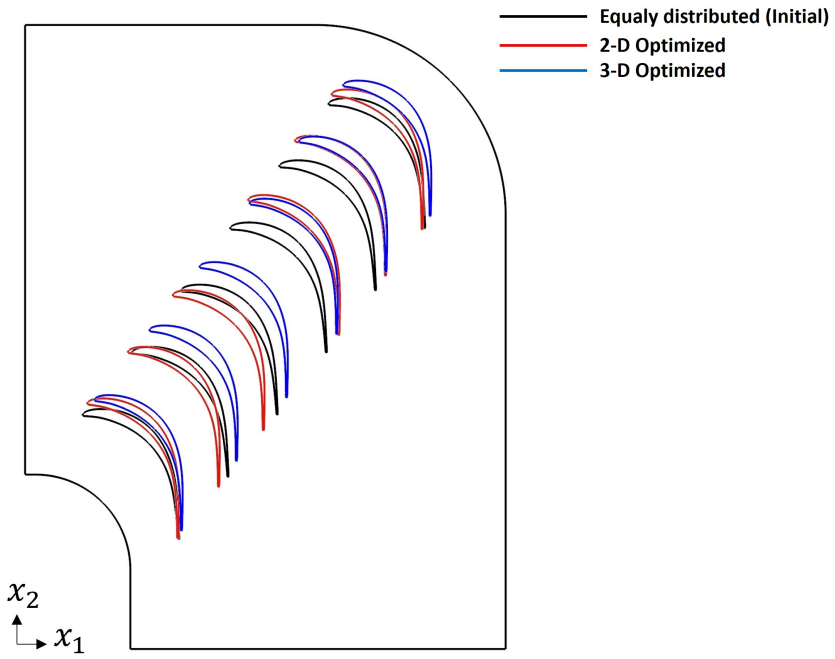

Figure 25: Vane Position Distribution comparison between Initial (Black Lines), 2-D Optimized (Red Lines) and 3-D Optimized (Blue Lines) Design

In Figure 26 below, the velocity distributions of five different three-dimensional designs have been analyzed. None of them exhibit any flow separation. The effects on the outlet velocity distribution can be observed, attributed to the varying positions of the guide vanes across the designs.

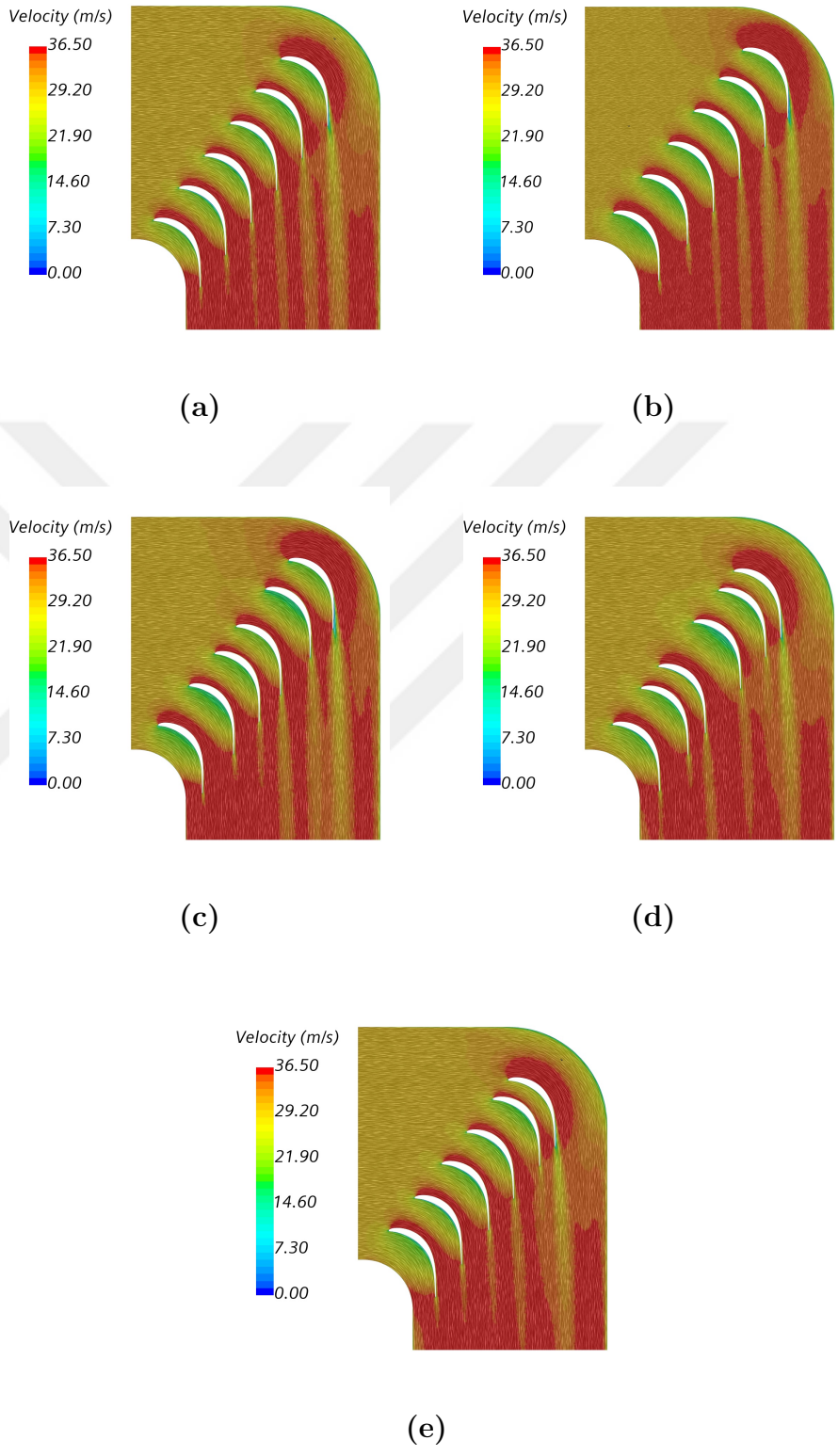

Figure 26: Three-dimensional velocity distribution scenes for various designs: (a) initial design, (b) optimum design, (c) optimum wall shear stress value design, (d) optimum gradient value design, and (e) optimum C_{loss} value design.

Minimizing sum of $\sum \left(\frac{\partial U_y}{\partial x}\right)^2$ and $\sum \left(\frac{\partial U_y}{\partial z}\right)^2$ on the outlet region were taken into consideration while minimizing $\sigma_{\tau_w} = \sqrt{\frac{1}{N}\sum_{i=1}^{N}(\tau_{wi} - \bar{\tau}_w)^2}$ on the outer wall. With this method, separations were eliminated and the outlet of the corner had a uniform velocity distribution. Secondary flow structures started to appear in the three-dimensional simulations. To address these structures, the secondary flow loss coefficient was reduced. These structures cannot be completely removed; their effects are reduced. A comparison of Figures 28a. and 28b. will show this minimizing of impacts. As C_{loss} was reduced, C_{SKE} was also decreased. As shown in Figure 27, the representation of the C_{loss} values at the outlet is presented. It is evident that the area indicated by the arrow represents the symmetry plane. Subsequently, C_{loss} values will be examined in relation to this area.

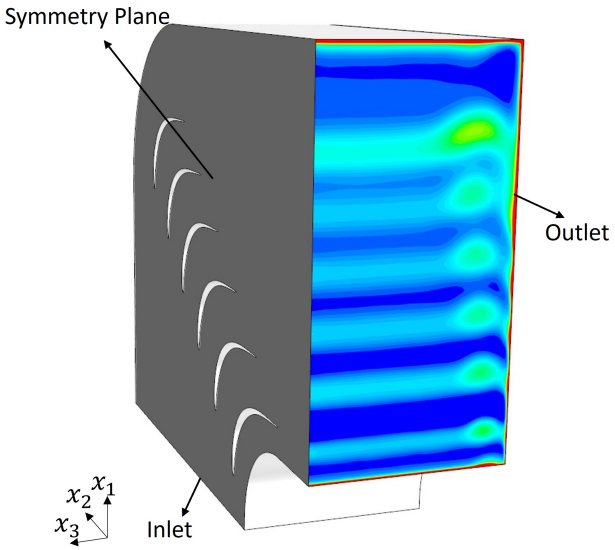

Figure 27: C_{loss} values and symmetry plane representation region

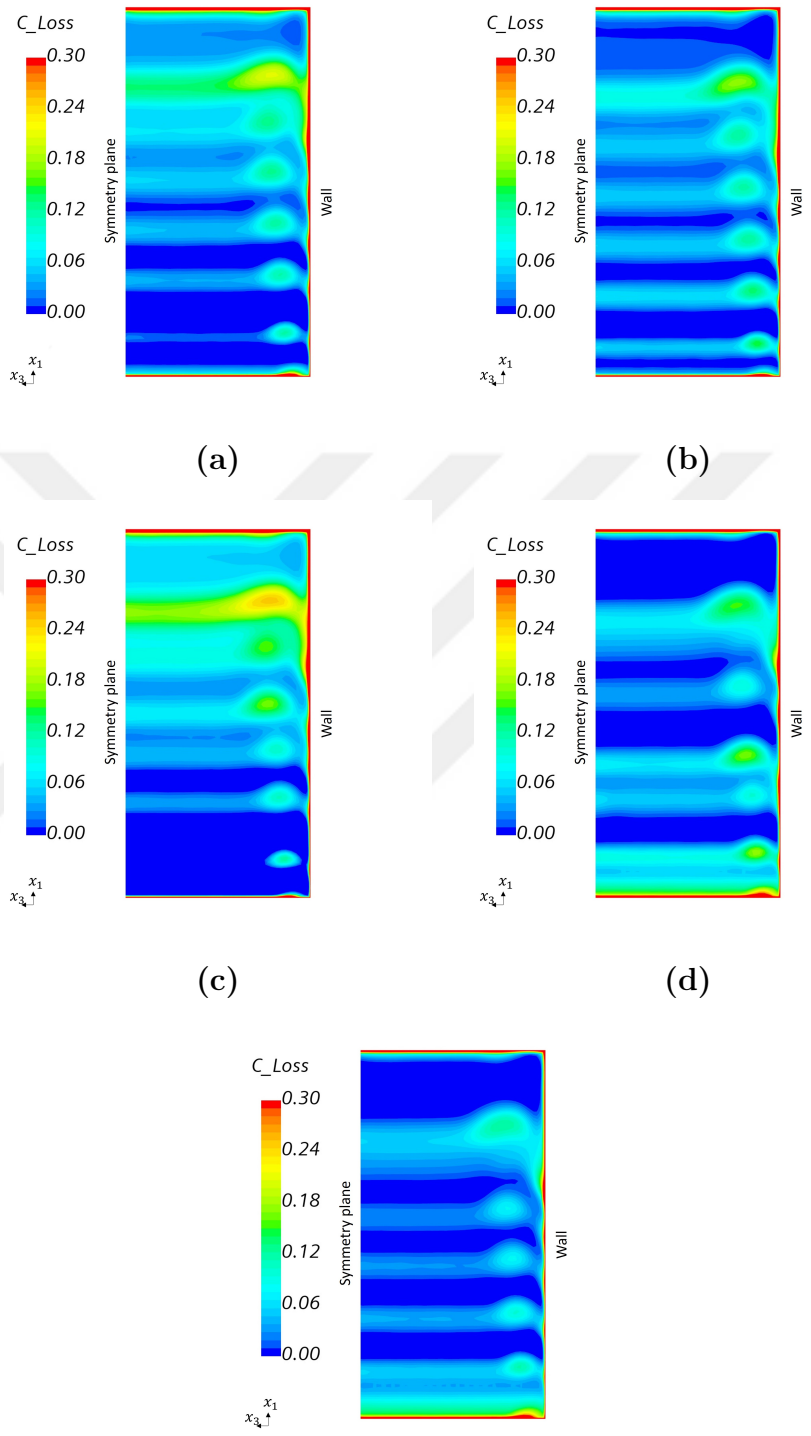

Figure 28: Three-dimensional C_{loss} values at the Corner Outlet for various designs: (a) Initial design, (b) Optimum design, (c) Optimum Wall Shear Stress value design, (d) Optimum Gradient value design, and (e) Optimum C_{loss} value design.

The primary flow direction is deviated from by secondary flows, which are caused by the curvature of flow channels and obstructions like airfoil guide vanes. These flows cause inefficiency and possible damage by increasing turbulence and wall shear stress. Maintaining a streamlined and effective flow requires minimizing secondary flow impacts.

As illustrated in Figure 29, the initial design shows the C_{loss} value at the threshold level. In contrast, Figure 30 demonstrates that the value decreases as a result of the optimization process. This reduction in C_{loss} also indicates a visible decrease in the effects of secondary flow.

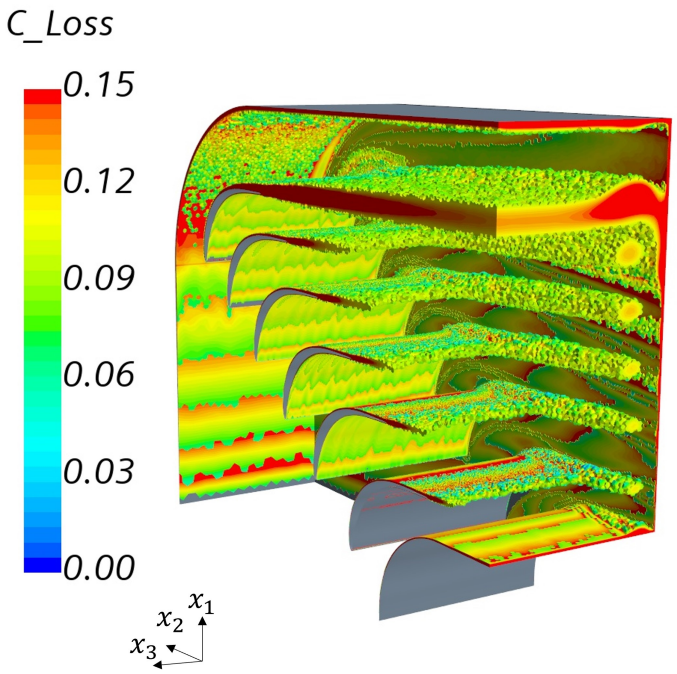

Figure 29: C_{loss} threshold values for initial design

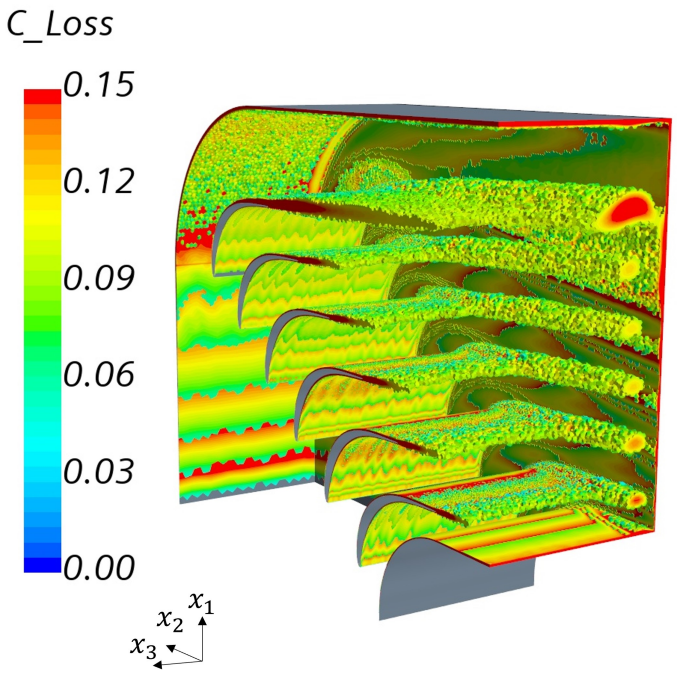

Figure 30: C_{loss} threshold values for optimum design

One of the main goals of this study was to decrease the wall shear stress standard deviation on the outer corner wall. By minimizing high-stress areas that might deteriorate materials and reduce efficiency, this method sought to provide a uniform wall shear stress distribution. Targets included minimizing secondary flow influences and achieving a uniform velocity distribution at the outlet through airfoil guide vane position optimization.

The standard deviation of the wall shear stress on the outer wall was minimized. As shown in Figure 31, the right side is defined and marked as the symmetry plane. The wall shear stress on the outer wall is illustrated in the scene, which will serve as a reference for further analyses.

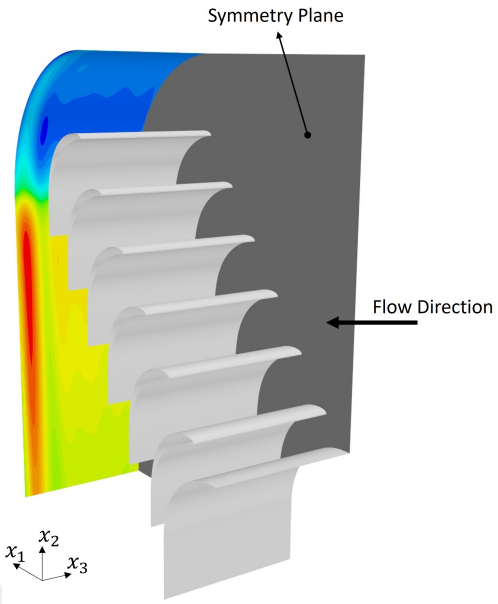

Figure 31: Wall Shear Stress values and symmetry plane representation region

The optimization outcomes, which are shown in the Figures 32, highlight how effective this strategy is. Significant secondary flow effects and areas of high shear stress were indicated by the first configurations' considerable variability in wall shear stress. On the other hand, the improved design validated the optimization approach by exhibiting decreased variability and the overall amount of wall shear stress. The modified guide vane placements resulted in a more equal velocity profile at the outlet, which ensures smooth flow and minimizes turbulence and secondary flows, as shown in Figure 32. Additionally, the reduced wall shear stress indicates a decrease in secondary flow effects, which results in reduced frictional losses and increased efficiency.

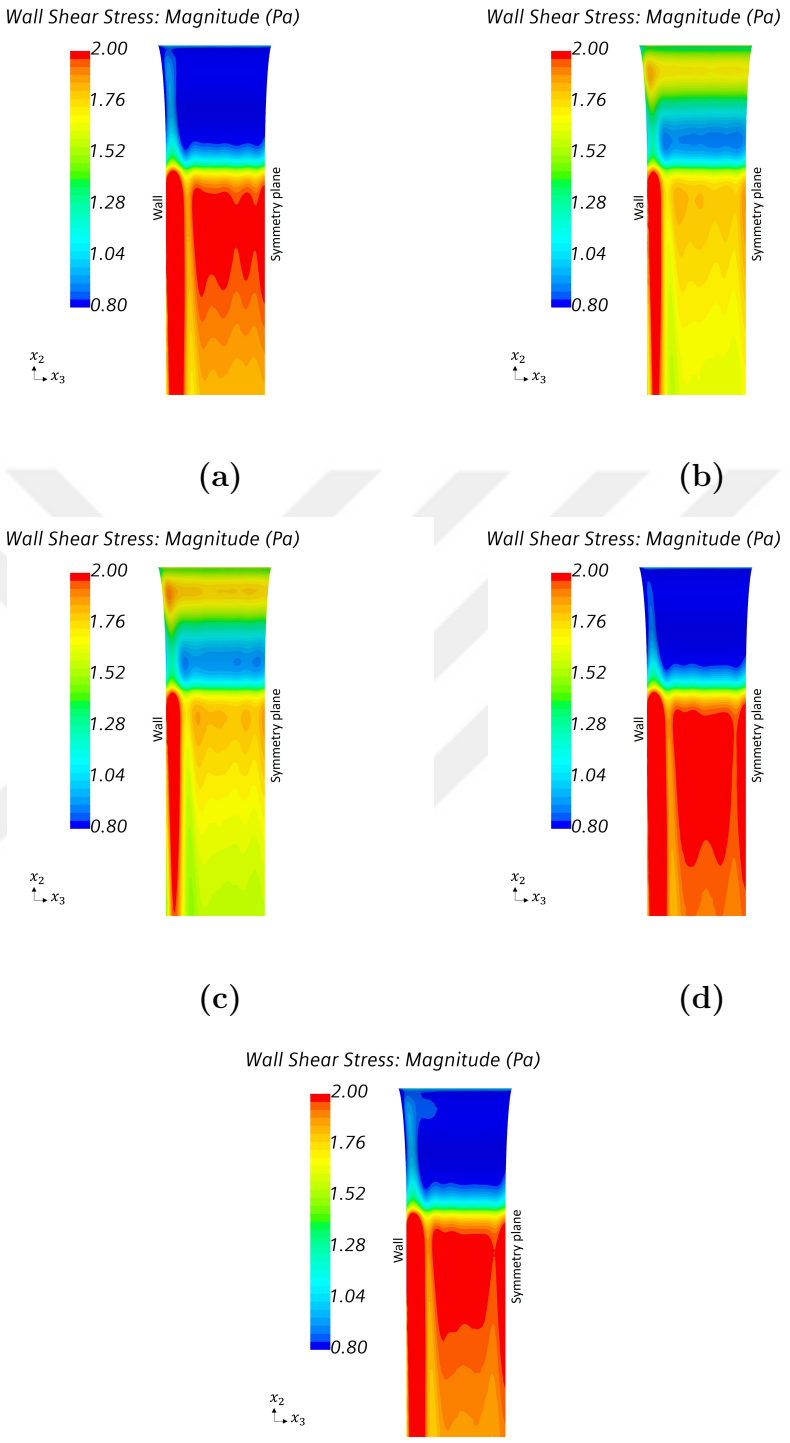

Figure 32: Wall Shear Stress values at the Corner Outlet for various designs: (a) Initial design, (b) Optimum design, (c) Optimum Wall Shear Stress value design, (d) Optimum Gradient value design, and (e) Optimum C_{loss} value design.

Achieving the appropriate flow characteristics has been shown to be significantly aided by the incorporation of wall shear stress as a critical optimization element. A uniform velocity distribution was attained at the outlet by minimizing the standard deviation of the wall shear stress, which also successfully decreased the impacts of secondary flow. These results emphasize how crucial it is to take wall shear stress into account when designing and refining guide vane systems. To further improve performance under various situations, future research might investigate real-time changes and adaptive vane designs.

It is clear from a close look at Figure 28b. that the secondary flow effects are amplified. When compared to alternative outlet flow distributions, a more uniform distribution does not always mean that the consequences of secondary flow are lessened. These impacts were reduced by using the minimization of C Loss values.

The coarse and fine mesh resolutions were compared. Figure 33 presents the velocity distribution at the outlet for the three-dimensional optimum results. It is observed that the velocity structures were accurately captured. Based on these structures, it is evident that conducting the optimization at a finer resolution would not have yielded significantly different results. As seen in Figure 34, the secondary flow structures become more pronounced with the fine mesh. The C_{loss} value of the initial design at fine resolution is shown in Figure 35 . The optimum design is still better than the initial design.

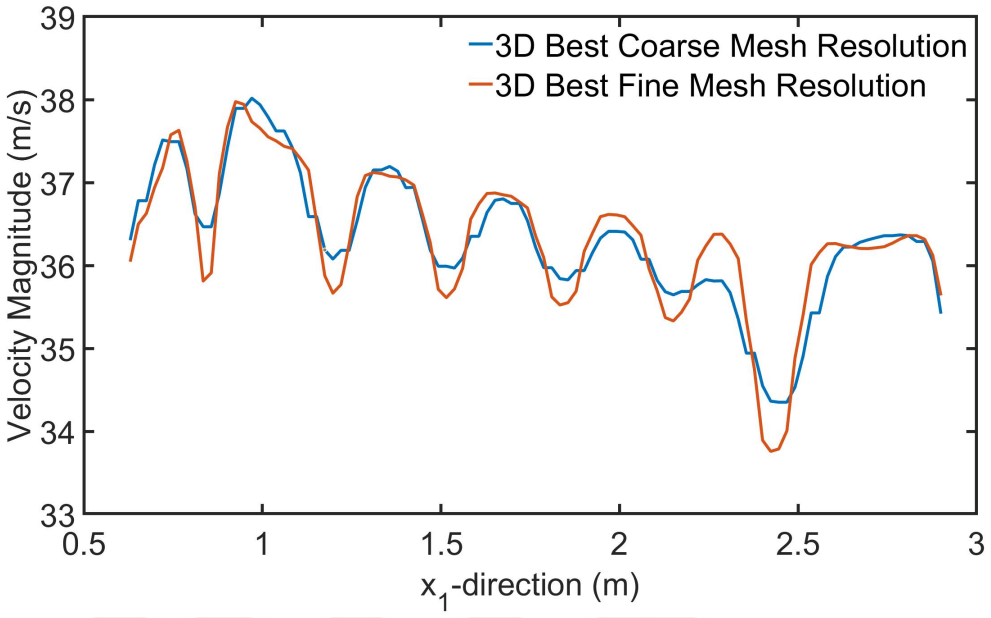

Figure 33: Three dimensional optimum design velocity distribution for coarse and fine mesh resolution(Left side is inner corner, Right side is outer corner)

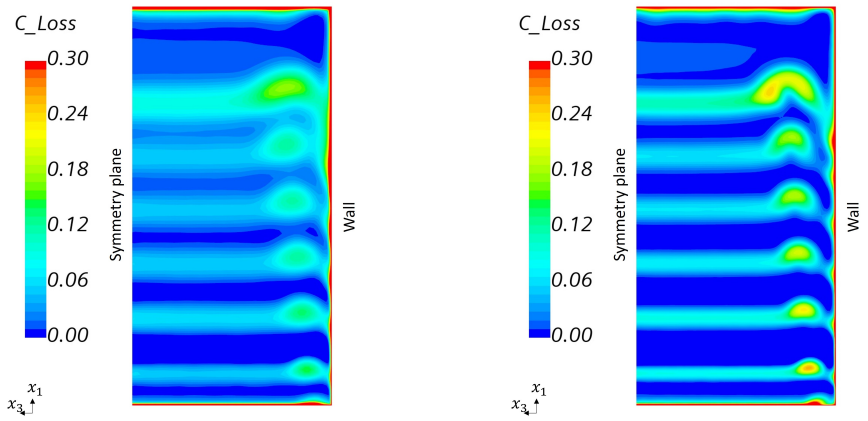

(a) **(b)**

Figure 34: C_{loss} value for optimum design with (a) Coarse mesh resolution, (b) Fine mesh resolution.

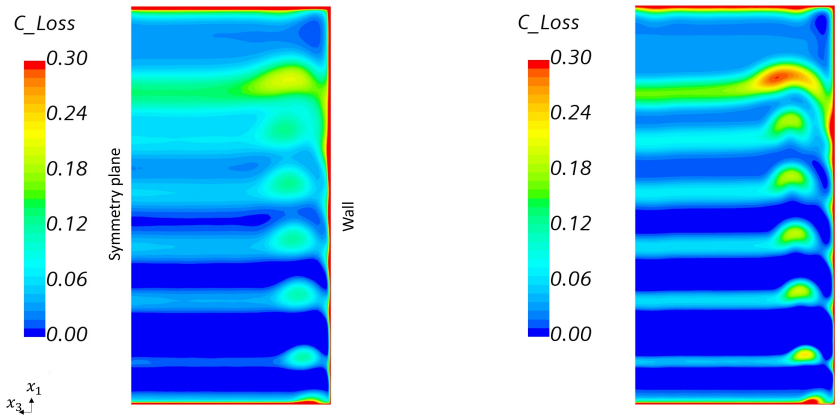

(a) **(b)**

Figure 35: C_{loss} value for initial design with (a) Coarse mesh resolution, (b) Fine mesh resolution.

CHAPTER V

CONCLUSION

In this study, CFD optimization was applied to achieve uniform velocity distribution and minimize flow separation in a wind tunnel corner. Initially, a two-dimensional optimization was conducted, focusing on adjusting the angle of the airfoil and the distance between the guide vanes. Two objective functions guided this process: the summation of the velocity gradient at the corner outlet, which ensured a uniform velocity distribution, and the minimization of the standard deviation of wall shear stress on the outer wall, which helped prevent separation. This phase successfully achieved a uniform velocity distribution at the outlet.

The successful two-dimensional designs then served as the seed for the subsequent three-dimensional optimization process. In this phase, secondary flow effects emerged, and the goal was to maintain a uniform velocity distribution while minimizing these effects. The objective functions were refined to include minimizing two different velocity gradient summations for improved uniformity and further reducing the standard deviation of wall shear stress to limit separation. Additionally, the C_{loss} coefficient was calculated and minimized to further reduce secondary flow effects.

The final design achieved a uniform velocity distribution with minimized secondary flow effects, specifically tailored for a contracting corner where flow accelerates. This study provides a new approach to reducing secondary flow effects and ensuring uniform velocity distribution in turning corners. The findings will aid future applications involving turning and the use of guide vanes by optimizing flow distribution and mitigating secondary flow impacts.

APPENDIX A

AIRFOIL GUIDE VANE COORDINATES

Table 9: Airfoil Suction and Pressure Surface Coordinates

Suction Surface		Pressure Surface	
x	y	x	y
1	0	0.004237	-0.01742
0.997759	0.002822	0.010071	-0.02066
0.992278	0.008003	0.014758	-0.01753
0.978297	0.018553	0.026027	-0.00502
0.953355	0.035135	0.044019	0.01593
0.918998	0.058109	0.069645	0.043607
0.875758	0.086957	0.104759	0.075179
0.82432	0.120635	0.149722	0.108436
0.765513	0.157406	0.203658	0.141761
0.699905	0.194603	0.265987	0.171925
0.627208	0.229335	0.336258	0.195895
0.547568	0.257397	0.412337	0.210621
0.462526	0.275319	0.491055	0.213411
0.374775	0.278719	0.569956	0.204677
0.290377	0.265453	0.645061	0.185164
0.213552	0.23701	0.713902	0.158172
0.147974	0.198267	0.776352	0.127814
0.094147	0.153249	0.831817	0.097507
0.053231	0.107504	0.879954	0.069415
0.024129	0.065106	0.920344	0.044907
0.006447	0.028486	0.952459	0.025007
0	0	0.989708	0.002279

REFERENCES

[1] M. Y. Jongtae Kim and S. Kim, "Characteristics of secondary flow induced by 90-degree elbow in turbulent pipe flow," *Engineering Applications of Computational Fluid Mechanics*, vol. 8, no. 2, pp. 229–239, 2014.

[2] M. González, A. Lopez, A. A., J. Perales, Y. Wu, and S. Xiaoxiao, *Design Methodology for a Quick and Low-Cost Wind Tunnel*. 03 2013.

[3] I. E. Idelchik, *Handbook of Hydraulic Resistance*. New York: Begell House, 4 ed., 2007.

[4] A. Pope and W. H. Rae, *Low-speed wind tunnel testing. –*. Wiley, 1984.

[5] R. R V, S. Son, A. Suryan, and H. Kim, "Study on reduction in pressure losses in pipe bends using guide vanes," *Journal of Visualization*, vol. 22, 05 2019.

[6] A. Abdelhamed, Y.-S. Yassen, and M. ElSakka, "Design optimization of three dimensional geometry of wind tunnel contraction," *Ain Shams Engineering Journal*, vol. 6, no. 1, pp. 281–288, 2015.

[7] R. Mehta and P. Bradshaw, "Design rules for small low speed wind tunnels," *The Aeronautical Journal*, vol. 83, no. 827, p. 443–453, 1979.

[8] L. Cattafesta, C. Bahr, and J. Mathew, *Fundamentals of Wind-Tunnel Design*. 12 2010.

[9] A. Sahlin and A. V. Johansson, "Design of guide vanes for minimizing the pressure loss in sharp bends," *Physics of Fluids A: Fluid Dynamics*, 08 1991.

[10] P. M. Ligrani, "A study of dean vortex development and structure in a curved rectangular channel with aspect ratio of 40 at dean numbers up to 430," Tech. Rep. NASA-19950005258, NASA, 1995.

[11] H. Takamura, S. Ebara, H. Hashizume, K. Aizawa, and H. Yamano, "Flow Visualization and Frequency Characteristics of Velocity Fluctuations of Complex Turbulent Flow in a Short Elbow Piping Under High Reynolds Number Condition," *Journal of Fluids Engineering*, vol. 134, p. 101201, 09 2012.

[12] H. Iacovides, B. Launder, and P. Loizou, "Numerical computation of turbulent flow through a square-sectioned 90° bend," *International Journal of Heat and Fluid Flow*, vol. 8, no. 4, pp. 320–325, 1987.

[13] J. Kreskovsky, W. Briley, H. McDonald, U. S. N. Aeronautics, S. A. Scientific, T. I. Branch, L. R. Center, and S. R. Associates, *Prediction of Laminar and Turbulent Primary and Secondary Flows in Strongly Curved Ducts*. NASA contractor report, National Aernautics and Space Administration, Scientific and Technical Information Branch, 1981.

[14] A. M. K. P. Taylor, J. H. Whitelaw, and M. Yianneskis, "Curved Ducts With Strong Secondary Motion: Velocity Measurements of Developing Laminar and Turbulent Flow," *Journal of Fluids Engineering*, vol. 104, pp. 350–359, 09 1982.

[15] Z. Yang and Q. Li, "Effects of reynolds number on wind tunnel corner losses," 01 2008.

[16] D. Apsley and M. Leschziner, "Advanced turbulence modelling of separated flow in a diffuser," *Flow, Turbulence and Combustion*, vol. 63, pp. 81–112, 04 2012.

[17] C. Hirsch, *Numerical computation of internal and external flows: The fundamentals of computational fluid dynamics*. Elsevier, 2007.

[18] D. C. Wilcox, "Formulation of the k-w turbulence model revisited," *AIAA Journal*, vol. 46, no. 11, pp. 2823–2838, 2008.

[19] F. R. Menter, "Two-equation eddy-viscosity turbulence models for engineering applications," *AIAA Journal*, vol. 32, no. 8, pp. 1598–1605, 1994.

[20] H. Schlichting and K. Gersten, *Boundary-Layer Theory*. Springer, 8th ed., 2000.

[21] H. Reichardt, "Vollständige darstellung der turbulenten geschwindigkeitsverteilung in glatten leitungen," *ZAMM - Journal of Applied Mathematics and Mechanics / Zeitschrift für Angewandte Mathematik und Mechanik*, vol. 31, no. 7, pp. 208–219, 1951.

[22] R. C. Technology, "Sherpa an efficient and robust optimization/search algorithm," *www.redcedartechnology.com*, 2017.

[23] G. Mingardo, "Secondary flow mitigation in turbine vanes through endwall fence shape optimization," *Aerospace Engineering*, 2015.

VITA

Aziz Mert Karul received his Bachelor of Science degree in Mechanical Engineering from Özyeğin University. He is currently pursuing a Master of Science degree in Mechanical Engineering at Özyeğin University. His areas of expertise include fluid mechanics, computational fluid dynamics (CFD), and CFD optimization.